Thesis for the Degree of Licentiate of Engineering

Characterisation of Optical Fibers Using Dual-Comb Swept-Wavelength Interferometry

Ekaterina Deriushkina

CHALMERS

Photonics Laboratory
Department of Microtechnology and Nanoscience - MC2
Chalmers University of Technology
Göteborg, Sweden, 2022

Characterisation of Optical Fibers Using
Dual-Comb Swept-Wavelength Interferometry
Ekaterina Deriushkina
Göteborg, May 2022

Chalmers University of Technology
Microtechnology and Nanoscience - MC2
Photonics Laboratory
SE-412 96 Göteborg, Sweden
Phone: +46 (0) 31 772 1000

ISSN 1652-0769
Technical Report MC2-454

Printed in Sweden by Reproservice, Chalmers University of Technology
Göteborg, Sweden, May 2022

Characterisation of Optical Fibers Using
Dual-Comb Swept-Wavelength Interferometry

Ekaterina Deriushkina
Photonics Laboratory
Department of Microtechnology and Nanoscience - MC2
Chalmers University of Technology

Abstract

The growth in data traffic coupled with trends in internet use will result in a requirement for interfaces of the network to reach Tb/s data rate in the future. Considering this, novel transmission techniques that can increase the date rate with orders of magnitude must be considered. One such example is space-division multiplexing (SDM) fibers. Application of novel fibers and SDM components in communication systems is always coupled with limitations and distortions of the signal due to crosstalk, dispersion, differential mode group delay (DMGD) and other effects. They can be calculated, studied and partially mitigated if the transfer function of the fiber under test is known. Thus, it is essential to characterize the fiber's and other component's transfer matrix using fast and accurate measurement techniques. Moreover, these characterisation measurements can be used for building channel models, which can assist in simulations of the transmission and estimation of ultimate system performance.

In this thesis various techniques for SDM devices characterisation are described and a novel method based on dual-comb spectroscopy and swept-wavelength interferometry is proposed and evaluated. The presented technique, dual-comb swept-wavelength interferometry (DC-SWI), is studied in terms of capabilities, advantages and limitations with application on different devices under test. This experimental scheme is also used for characterisation of a coupled-core fiber, where the transfer function and DMGD values were extracted.

Furthermore, different channel models describing the properties of SDM fiber links are briefly reviewed and discussed.

Keywords: characterisation measurements, swept-wavelength interferometry, dual-comb spectroscopy, transfer function, coupled-core multi-core fibers, channel modeling.

Publications

This thesis is based on the work contained in the following papers:

[A] **Ekaterina Deriushkina**, Israel Rebolledo-Salgado, Mikael Mazur, Victor Torres-Company, Peter Andrekson, Simon Gross, Michael J. Withford, Tetsuya Hayashi, Takuji Nagashima, Jochen Schröder, and Magnus Karlsson, "Characterisation of a Coupled-Core Fiber Using Dual-Comb Swept-Wavelength Interferometry", in *European Conference on Optical Communication (ECOC)*, Bordeaux, France, Sep 2021.
DOI: 10.1109/ECOC52684.2021.9605879

[B] **Ekaterina Deriushkina**, Israel Rebolledo-Salgado, Mikael Mazur, Victor Torres-Company, Peter Andrekson, Jochen Schröder, and Magnus Karlsson, "Dual-Comb Swept-Wavelength Interferometry: Theory and Experiment", *Journal of Lightwave Technology*, in review.

Other publications by the author, not included in this thesis, are:

[C] Krishna Twayana, Israel Rebolledo-Salgado, **Ekaterina Deriushkina**, Jochen Schröder, Magnus Karlsson and Victor Torres-Company, "Spectral interferometry with frequency combs", *Micromachines*, vol. 13, no. 4, 614, 2022.
https://doi.org/10.3390/mi13040614

Contents

Acknowledgement

First and foremost, I would like to thank my supervisors, Prof. Magnus Karlsson and Dr. Jochen Schröder, for giving me the opportunity to start my journey to PhD and guiding me throughout the scientific terrain. Thank you for always having your doors open and teaching me thousands of interesting and important things. I am grateful to Prof. Peter Andrekson for being such a responsible examiner and chief, always motivating and helping me. I also want to thank my co-superviser, Prof. Erik Agrell, and all the researchers and students from KAW Dimensions project. I wish to thank Prof. Mikael Fogelström for great support and excellent organisation of the work in MC2.

My big thanks goes to Prof. Victor Torres Company for always giving excellent explanations and enlightening the subject matter of the comb spectroscopy. Israel Rebolledo-Salgado deserves many thanks for making me to understand the dual-comb spectroscopy basics and general lab stuff. I highly appreciate your participation in my work! Thank you, Krishna Sundar Twayana, for the time that you devoted to explaining me the swept-wavelength interferometry technique. I would also like to show gratitude to Dr. Mikael Mazur not only for his great participation and help that is highly appreciated, but also for inspiring and motivating me. I am grateful to Dr. Kovendhan Vijayan who shared his excellent knowledge and helped in the lab all the time and Dr. Ping Zhao who is always very friendly and helpful if some issues occur. My big thankfulness is to Alexander Caut for teaching me a lot of stuff about Canvas and having interesting discussions not always related to science. I want to thank Prof. Åsa Haglund for encouraging me to follow my future goals.

I am also thankful to all people in Photonics lab for sharing interesting insights and having nice talks.

I am grateful to Jeanette Träff, Gunnel Berggren, Debora Perlheden and Susannah Carlson for being so nice and professional administrators who make significant work. Thank you, Jeanette, for all your help in my first days in Gothenburg.

I am very thankful to my dear friends who supported me during these years, colored my days and besides the scientific issues also shared some personal parts of their life with me. Special thanks is to Zonglong He, who has such a brilliant mind and with whom I am so proud to work. Ali Mirani became not only my very good friend, but also a guide in a world of modulation formats. Rasmus Larsson deserves a "stort tack" for sharing his knowledge not only on PSA and optics, but also about the Swedish language, orienteering and nice music. I am also thankful to Oxana Ahlström (Lubchenko), Dr. Roman Skoryunov, and Eduard Yakupov whose great support and participation are just invaluable throughout my life in Russia and Sweden. I am so grateful for these friendships and that all of you always have been sincere, honest and supportive.

I also want to thank my karate sensei Christian Olausson for sharing treasured knowledge and skills. Very special thanks to Joakim Holmlund for giving me a rental contract in one of the most beautiful places in Gothenburg (and in the world!) and for always being helpful. I appreciate a great work of my language teachers Dr. Zahia Bouaissi, Davide Gemello, Roberto Mendez, Dr. Anna Oveshkova and Kristina Mamayusupova, thanks to whom I improved my skills and had really great time during these years. I am grateful to Marcello Girardi for having very interesting conversations with me, particularly in Italian language. Muchas gracias to Estrella Torres for bringing a lot of joy and support and for having conversations in Spanish with me. I also thank Linda Brånnel for playing a huge role in my Swedish language improvement and for helping me to settle down in Gothenburg.

I want to express acknowledgement to my school physics teacher, Yury Basargin, and university professors Evgeny Pamyatnykh, Yury Panov, Irina Bostrem and Vladimir Malishev for being excellent teachers and supervisors and showing me an exciting world of science. Prof. Eugene Kogan deserves my gratitude for teaching me the most important lessons and sharing his scientific experience. Thanks to Dr. Anna Klepikiova for supporting me in my scientific findings and for believing

in me. Big thanks goes also to Mikhail Popov, Dr. Natalia Urusova, Anton Firsin and Alexander Saveliev.

I must express my very profound gratitude to my family. I want to thank my mother and father, Oxana and Vladimir Ilchenko, for encouraging my passion to science and life choices. I am especially grateful to my sister, Maria Ilchenko, who has always been curious about the world and shared her dreams and thoughts. Thank you for your love and endless support. I am so proud to have such a nice mother-in-law, Lubov Deriushkina, whose great wisdom and joy assisted me during this time. Finally, huge and very special gratitude to my husband, Vsevolod Deriushkin. This work would not be possible without your continuous love, support and trust.

Ekaterina Deriushkina
Göteborg, May 2022

Acronyms

ADC	analog-to-digital converter
AOM	acousto-optic modulator
CCF	coupled-core fiber
DAQ	data acquisition
DCS	dual-comb spectroscopy
DS-SWI	dual-comb swept-wavelength interferometry
DGD	differential group delay
DMGD	differential mode group delay
DSP	digital signal processing
DUT	device under test
EDFA	erbium-doped fiber amplifier
FC	frequency comb
GVD	group velocity dispersion
MCF	multi-core fiber
MDL	mode-dependent loss
MMF	multi-mode fiber
MIMO	multiple-input and multiple-output
PMD	polarization mode dispersion
SDM	space division multiplexing
SNR	signal-to-noise ratio
SWI	swept-wavelength interferometry

CHAPTER 1

Introduction

1.1 Motivation

Optical fibers and photonic devices are central to modern communication links and also have applications in other areas like medicine and metrology. Since the development of the first optical fibers and their application in gastroscopy [1] and data transmission [2] it was relevant to characterise their parameters. Characterisation measurements assist in estimation of the device quality, its manufacture process and can give a clue of how the investigated properties can be improved.

The purposes of characterisation experiments are not limited only to quality control. Even if the manufacturing process resulted in photonic devices of extremely high quality, there are still other features that can be measured and that may provide information about the device, such as coupling coefficients, higher order dispersion, mode-dependent loss (MDL) or differential group delay (DGD). All such parameters can be extracted from the transfer function, which describes how the output of the system is connected with its input. In other words, if the transfer function of the device under test (DUT) can be measured, almost all linear parameters of interests can be easily extracted. Moreover, results of such measurements can contribute to channel models which can be beneficial in simulations and further improvements of the optical links. In fact, the channel model is crucial in communication theory for esti-

mating the performance of a communication channel. More specifically, the channel capacity, i.e., the maximum data rate that can be transmitted error-free over a channel, depends solely on the channel model, as pioneered by Shannon in 1959 [3].

Since the demands on the data throughput have risen intensely, space division multiplexing (SDM) components gained a lot of interest in terms of increasing the data capacity. There are three general approaches in SDM: multiple independent cores inside a fiber (multi-core fiber (MCF)) [4], transmission through several modes of a multi-mode fiber (MMF) [5] and the use of fibers with few strongly coupled cores [6]. All mentioned types of fibers have their advantages and limitations and have been applied in different scenarios. Transmission through all of them, however, is coupled with complex effects that impair a propagation and can make the link design and digital signal processing (DSP) complicated. This further highlights a relevance of developing high-precision characterisation techniques that can assist in extraction of these impairments and creating realistic channel models.

1.2 History

The history of optical fiber characterisation measurements most likely started in 1970, when Kapron with coauthors from Corning published a seminal work on low-loss silica fibers, and measurement of losses in those [7]. Another key parameter for fiber characterisation was dispersion since it limited the transmission reach and one of the first works where it was characterised dates back to 1973, where the authors extracted the pulse dispersion by injecting short impulses of light into a fiber and measuring the temporal pulse spread at the output [8]. The pulse dispersion versus length was then measured as a step in a quality control after the manufacturing [9] using a shuttle pulse technique [10]. At the same time, experiments for extraction of material dispersion in 700-930 nm [11] and 1064-1550 nm [12] wavelength ranges by the time of flight (pulse delay) technique were established. The method is based on injecting pulses of different wavelengths into a fiber and measuring the change in temporal separation between the pulses after they have propagated through the fiber. Throughout the years the time of flight method using fiber Raman lasers [13], discrete-wavelength laser diodes [14], supercontinuum-radiation sources [15] and tunable soliton sources [16] has been applied for characterisation of photonic devices.

Today the time of flight technique is also extensively applied for transfer matrix characterisation [17] and included in methods recommended by the International Telecommunication Union for dispersion measurements alongside with phase-shift [18] and interferometric techniques [19].

With developing of optical modulation technologies, other techniques for dispersion characterisation arose. The chirp parameter and chromatic dispersion were measured in the frequency domain with small modulation depth, where sharp resonance frequencies originating from interferences between carrier and sideband wavelengths appear [20]. Another type of technique implied applying modulation instability sideband generation for dispersion and nonlinear coefficient extraction [21]. A method based on the phase mismatch of four-wave mixing was developed in the work [22] and demonstrated dispersion measurements with an accuracy of 0.03 ps/nm/km.

All the discussed techniques would not be possible without the invention of the laser [23]. In 1960 the first ruby laser was launched by Maiman [24] and one year later, the first continuously operating gas laser was invented [25] at Bell Labs. A few years later, in 1964, the first mode-locked laser that emitted ultrashort pulses was constructed by Hargrove and collaborators [26]. In the optical frequency domain such a laser represented a sequence of discrete lines that were equally spaced manifesting a comb-like structure. This formation was called a frequency comb (FC) and since 1964 the interest in FCs has led to remarkable research and inventions, particularly in the context of the dual-comb spectroscopy (DCS), which will be described in more detail in section 2.4. This technique has been very popular and applied for characterisation measurements not only in photonics [27] but also for liquid [28] and gas samples [29]. Another early example of comb-based fiber characterization is [30], where a dual-quadrature detection scheme based on polarization demultiplexing was used to characterize the dispersion of the fiber under test. The DCS was also combined with phase-sensitive optical time-domain reflectometry for temperature and strain change characterisation in fibers [31] and with single-pixel-imaging for optical vortex characterization [32]. In terms of SDM, the DCS was recently applied to characterise 110-km coupled-core fiber (CCF) [33]. Other applications dual-comb interferometers include spectroscopy [34], vibrometry [35], and imaging [36].

Another key technology in this context is tunable lasers. In 1966 the first tunable laser pumped by a ruby laser was invented by Mary L.

Spaeth of Hughes Research Labs and in 1980s came the arrival of semiconductor diode lasers that could be tuned using temperature or injection current. These lasers enabled a huge progress in telecommunications, but also provided novel experimental opportunities in terms of characterisation of photonic devices. For example, the Poincaré sphere [37] and the Jones matrix [38] methods for measuring polarization mode dispersion (PMD), one of the principal impairments in optical fibers.

In 1980s there appeared a set of techniques that being united under the basis of Swept-wavelength interferometry (SWI). One of the first techniques were described in 1981 by Eickhoff and Ulrich [39] and was called optical frequency domain reflectometry (OFDR). Since that time OFDR systems have been developed to characterise fiber-optics networks and components [40, 41] and were employed to measure strain [42], temperature [43] and vibration [44]. Other SWI techniques include FMCW ladar (laser detection and ranging) [45] and swept-source optical coherence tomography, which has been highly successful in measuring biological samples, such as skin [46]. In SDM devices characterisation it is usual to extend SWI with the configuration called optical vector network analyzer (OVNA). Recent progress show that this technique is successful in transfer function extraction for few-mode fibers [47, 48], MMFs [49], deployed SDM fibers [50] and spatial multiplexers [51, 52].

Another important breakthrough in characterisation techniques happened in 1948 when Denis Gabor [53] invented holography, a method which enables capturing both amplitude and phase of an object by utilizing the interference of light. A medium containing this information is called a "hologram" [54]. A 3D image can be then reconstructed from a hologram by using the theory of diffraction of light. Digital holography (DH) [55] that was developed in 1960s is a technique in which a digital hologram that contains an object wavefront is recorded, and both 3D and quantitative phase images of an object are reconstructed using a computer. This developments enabled many applications, which are reviewed in [56] and during last several years DH became one of the common techniques for characterisation of SDM devices and has been applied to characterise fibers with high mode count [50], photonic lanterns [57] and multimode erbium-doped fiber amplifier [58].

1.3 This thesis

The focus of this thesis is on characterising the full transfer function of SDM fibers for building a channel model from the measured transfer matrix. For this purpose we designed a technique, which combines the DCS that is based on the frequency combs and SWI, where a tunable laser source is used. The established technique, dual-comb swept-wavelength interferometry (DC-SWI), gains advantages and flexible trade-offs from both DCS and SWI.

The papers included in this thesis mark the benefits of the proposed experimental technique and demonstrate the results on transfer function characterisation. In [Paper A], transfer function characterisation of a three coupled-core fiber (3CCF) was performed using DC-SWI. The root mean square (RMS) widths of the impulse responses and differential mode group delay (DMGD) values were estimated for every core. [Paper B] is devoted to the comprehensive description of the DC-SWI technique. The operation principle, experimental implementation, DSP, performace characteristics, advantages and limitations were discussed in detail.

1.3.1 Thesis outline

The outline of this thesis is as follows. In chapter 2, various SDM-focused characterisation techniques, their advantages and limitations are discussed. In chapter 3, the DC-SWI technique is introduced and its features and capabilities are explained in detail. Chapter 4 overviews the channel models for SDM. Finally, in chapter 5, the future outlook is presented and chapter 6 outlines the main results in the appended papers.

CHAPTER 2

Characterization of SDM devices

Characterization of optical fibers and photonic devices is extremely important for quality control and gaining principal information for the fiber optical links and their improvement. This requires application of accurate and sensitive measurement techniques capable of retrieving the parameters of interest. Some of the most important characterisation techniques were highlighted in the introduction chapter. The main focus of the thesis is a characterisation technique which is based on DCS and SWI, hence, description of these experimental methods is presented comprehensively. However, this chapter also includes an overview of other spatial and temporal SDM characterisation techniques.

2.1 Propagation effects in SDM devices

This section presents a brief description of various impairments present in transmission through SDM fibers that are of importance in characterisation and which should be accounted for in channel modeling. These effects can be linear or nonlinear. The former includes attenuation and different types of dispersion, which will be introduced in this section. The latter can be index-related, meaning Kerr nonlinearities subdivided into self-phase modulation, cross-phase modulation and four-wave mixing, or scattering-related comprising stimulated Brillouin scattering and stimulated Raman scattering. These nonlinear effects are summarised

in [59] and will not be discussed in this section since it is out of scope of this thesis.

2.1.1 Attenuation

Fiber loss per unit length is described by the attenuation coefficient α. Attenuation is wavelength-dependent and has two main contributions: Rayleigh scattering at short wavelengths and absorption at long wavelengths. Around 1550 nm, the sum of their terms is the lowest and the loss typical values are $\alpha \approx 0.2$ dB/km [60]. The power evolution of the optical field in the fiber is dictated by the Beer-Lambert law:

$$P(z) = P(0)e^{-\alpha z}, \tag{2.1}$$

where z is a propagation distance, $P(0)$ is a launched power and α is attenuation in linear units.

Rayleigh scattering happens because the refractive index changes due to microscopic variations in material density of the glass, leading to scattering. Absorption appears at longer wavelengths when silica molecules absorb more photons, causing attenuation. Additionally, bending losses can be a significant contribution to accumulated attenuation. If a fiber is bent tightly, light moves more to the edge of the core until it is not fully guided any more and starts becoming lossy. This type of loss sets a critical bend diameter found in data sheets of fibers.

The attenuation can be compensated using erbium-doped fiber amplifier (EDFA). However, these amplifiers add the noise caused by amplified spontaneous emission [61]. The noise figure in an ideal EDFA is 3 dB due to quantum limit [61], while practical amplifiers can have noise figure as large as 6-8 dB.

2.1.2 Group velocity dispersion

Group velocity dispersion (GVD) or chromatic dispersion is a linear propagation effect that appear owing to the group velocity is different for different frequency components in the optical fiber. Fiber-optic communication systems are affected by GVD since the waveform generated by the transmitter is distributed over different frequencies during the transmission inside the fiber. These frequency components propagate through the fiber with different velocities resulting in time domain pulse broadening [62] and although spectral components are launched into the fiber

at the same time, they have different transit times and will thus arrive at the receiver at different times.

Chromatic dispersion is characterised by the dispersion parameter D [ps/nm/km] which gives the pulse broadening per nm of spectral width per km of fiber. It can be described in terms of the propagation constant $\beta(\omega)$:

$$D = -\frac{2\pi c}{\lambda^2}\beta_2, \tag{2.2}$$

where λ is the wavelength, c is the speed of light and β_2 is a term in Taylor expansion of the propagation constant $\beta(\omega)$ that is proportional to its second derivative with respect to frequency evaluated at the carrier frequency ω_0 as $\beta_2 = \frac{\partial^2\beta}{\partial\omega^2}|_{\omega=\omega_0}$.

In single-mode fiber (SMF) links the GVD is static and can be compensated by introducing dispersion compensating fibers or by receiver DSP in case of coherent detection. Thus, it is not a central problem in transmission or channel modeling, unless it is imperfectly compensated.

2.1.3 Modal dispersion

The light propagating in multi-mode optical fibers must be analysed in the modes separately. The set of modes, their effective index and group velocity depend on the waveguide geometry. If a pulse is transmitted in one of the fiber modes, the group velocity defines how fast this pulse propagates. Modes in the optical fiber have different spatial profiles and can have different group velocities. If, for instance, the group velocity for one mode is larger than for another, a pulse exciting both modes will be dispersed and potentially split during propagation along the fiber. This phenomenon is called modal dispersion or intermodal dispersion.

One of the form of modal dispersion is PMD, where two different polarization modes of the light in a waveguide propagate at different speeds due to random imperfections breaking the circular symmetry [63]. This results in separation of the signal's polarization components causing spreading of pulses and as for all dispersion effects, the pulse broadening will lead to intrapulse crosstalk that will cause signal distortion and limit the available bandwidth of the channel unless it is compensated.

The strength of modal dispersion can be defined by time delay per unit length, which is inverse to the group velocity. This delay is referred as DGD, DMGD or differential mode delay (DMD), depending on a specific case and can be compensated by combining fibers with positive and

negative DGD [64, 65]. The principle is to offset the DGD introduced by a certain fiber by a very similar fiber with DGD of opposite sign. However, any mode coupling during transmission deteriorates the compensation and DMD-compensated links often have broadened impulse responses.

The modal dispersion effect is, if static, not necessarily detrimental for coupled SDM systems since multiple-input multiple-output (MIMO) DSP [66] enables compensation for any mixing. Moreover, the mixing can be even desirable in coupled SDM systems since in the regime of strong coupling DGD accumulates only with the square root of distance [67]. However, the random mode coupling that arises in MMF and CCF make modal dispersion random as well and varying with time. Modal dispersion, thus, requires adaptive equalizers [68] to be compensated and this is challenging if the modal delays are big and the drift is fast.

2.1.4 Mode-dependent loss

Imperfect coupling in SDM components can lead to different loss in different modes, which results in MDL and may also deteriorate the transmission performance [69, 70].

In an ideal system without MDL the transfer matrix of an SDM device is unitary. MDL, therefore, is described by non-unitary transfer matrices [71]. Using eigenvalue analysis or singular value decomposition, MDL can be then calculated as the ratio between the modulus of the maximum λ_{max} and minimum λ_{min} eigenvalues of the measured transfer matrix, i.e.,

$$MDL_{dB} = 10 \cdot \log_{10} \left[\frac{|\lambda_{max}|^2}{|\lambda_{min}|^2} \right]. \tag{2.3}$$

2.2 Spatially and spectrally resolved imaging

Spatially and spectrally resolved imaging (S^2) was first demonstrated in 2008 [72] and applied for imaging higher-order-modes propagating in large-mode-area fibers. The modes that propagate in optical fibers can be identified by both the group delay difference which leads to a spectral interference pattern for a broadband source propagating through the fiber, and a spatial interference pattern between the high-order modes and the fundamental mode [72]. In a MMF, the guided modes propagate

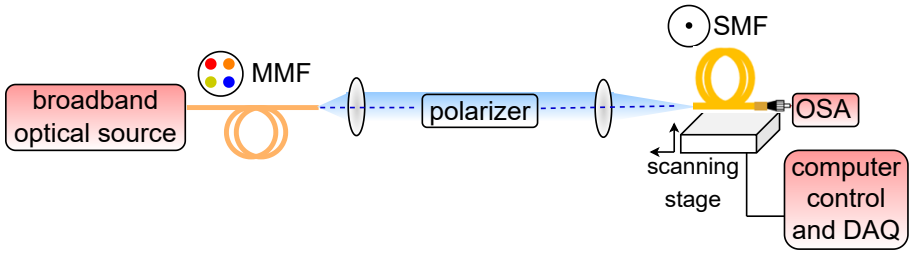

Figure 2.1: Experimental setup for S^2 imaging implementation from [72]

with a different speed and spectrally interfere. This results in the impairment called multi-path interference (MPI) and can lead to signal fading on a slow time scale [73]. The interference period of the MPI is connected with the DGD between the two interfering modes. The principle of S^2 imaging is based on measuring the MPI at several spatial points across the transmitted optical beam using a scanning fiber probe. The Fourier analysis of the recorded spectra assists in resolving the DGD between two interfering modes and retrieving the corresponding mode profiles.

Figure 2.1 shows the experimental setup for S^2 imaging implementation that was used in [72]. The light from a broadband optical source is launched into a MMF under test. The beam from the output of the fiber is imaged with magnification on the end of a SMF, which is then connected to an optical spectrum analyzer (OSA). A polarizer is needed in order to ensure that polarization states of the modes are aligned on the SMF end-face. The measured optical spectra are Fourier transformed and intensity profiles of the individual modes are extracted. The MPI can be calculated as a ratio of powers of the modes that can be found by integration of intensities over the fiber cross section.

Applications of S^2 imaging include mode analysis not only of large-mode-area MMFs [72, 74], but also photonic crystal fibers [75], all-solid and hollow core band-gap fibers [76], as well as extended long tapers [77] and silicone waveguides [78]. It has also been successfully applied to observe supermodes in a coupled few-mode three-core fiber [79], measure higher order mode bend-loss in photonic band-gap fibers [80], characterize efficient higher order mode suppression in scalable output fiber amplifiers [81]. Moreover, S^2 imaging technique was applied in a combination with correlation filter mode analysis for characterisation of optical fibers [82] and such a method provided simultaneous decomposition of one beam with considerable improved accuracy.

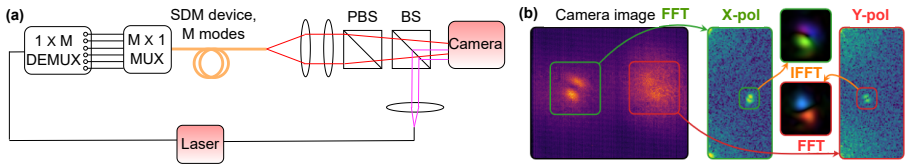

Figure 2.2: (a) Experimental setup for DH implementation. (b) Example of the DSP from [83].

2.3 Digital holography

Digital holography (DH) is a widely-used imaging method with a lot of applications. In terms of optical fiber characterisation, the use of DH can bring a lot of advantages, especially when a fiber with high mode count and strong coupling is considered [50, 83–85]. Compared to S^2 imaging that can fail in case of strong mode mixing, DH is more accurate since it acts as a perfect mode demultiplexer [50, 83].

Figure 2.2(a) demonstrates an example experimental setup that can be installed for characterisation, where a signal from a DUT beats with an angled reference beam on a camera. The light from an SDM device is imaged with magnification using a free-space optical setup. The interference between DUT signal and reference lead to fringes in optical intensity, which are captured by the camera.

An example of the recorded camera frame taken from [83] and further DSP process is presented in Fig. 2.2(b). First, a part of the image is cropped around the center of interference pattern. Next, these parts can be converted to the angular domain by Fourier transforming. Converted interference pattern needs to be filtered in the angular domain following a similar algorithm, so a new square piece of image has to be cropped. The filtered pattern is shifted back to spatial domain using the inverse Fourier transform. The resulted optical field contains both amplitude and phase information making it possible to calculate a complex transfer function of a a SDM-DUT.

2.4 Dual-Comb Spectroscopy (DCS)

Dual-Comb Spectroscopy (DCS) projects the information about a DUT from the optical to the RF domain, when two optical FCs of slightly different repetition rates interfere. The DCS is capable of simultaneous measurements of broadband and high-resolution spectra within microsec-

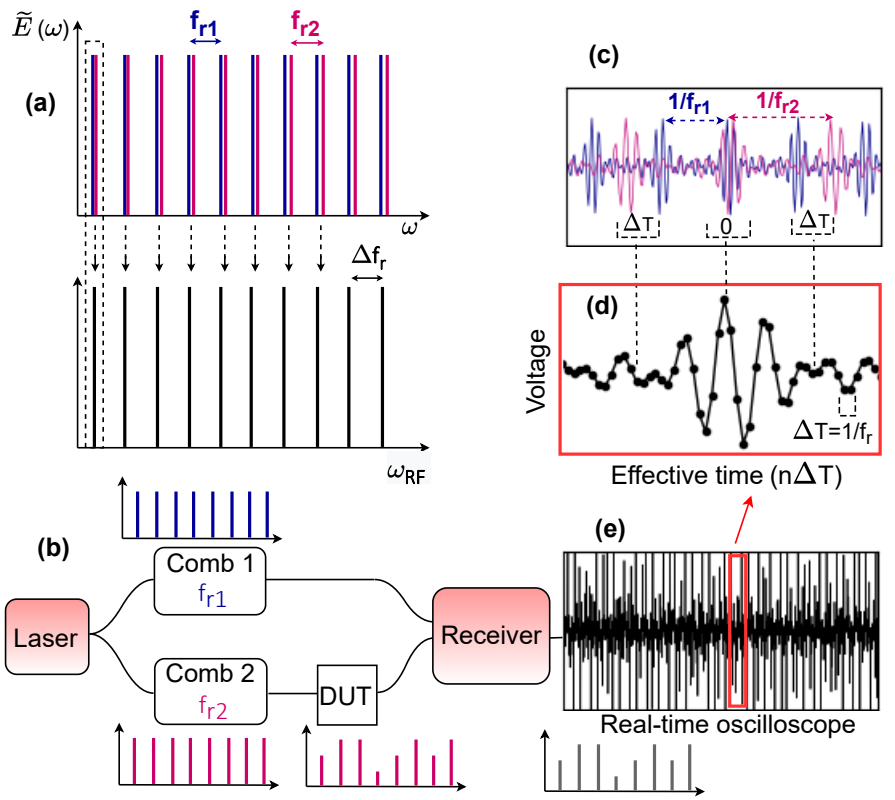

Figure 2.3: (a) Frequency domain representation of DCS. (b) Principle of DCS. (c), (d) Time domain representation of DCS for the (c) optical signals and (d) electric signal. (e) Captured interferogram.

onds. It is also characterised by high signal to noise ratio (SNR), high sensitivity, fast acquisition speeds, a small footprint, and implementation free of moving parts. Recent reviews on DCS can be found in [86, 87] and [Paper C]. In this section a brief overview of the operation principle, mathematical description, implementation alternatives and key experimental results on the use of DCS in photonic device characterisation is provided.

2.4.1 Operation principle

The operation principle of DCS can be explained in both frequency and time domains. In the frequency domain two FCs with slightly different repetition rates, f_{r_1} and f_{r_2}, interfere on a photodiode generating an RF

comb with a repetition frequency $\Delta f_r = f_{r_1} - f_{r_2}$ formed by heterodyne beating between pairs of optical comb teeth (Fig. 2.3(a)). At least one FC has to pass through the DUT, the frequency response of which changes the shape of the FC (Fig. 2.3(b)). The resulting absorption and phase on the comb teeth are modified into the corresponding amplitude and phase of the measured RF comb. The RF comb spectrum can also be extracted by Fourier transforming a set of time domain interferograms captured by the real-time oscilloscope (Fig. 2.3(e)).

In time domain two pulse trains with slightly different repetition rates interact and "walk through" each other (Fig. 2.3(c)). The resulting beating on a photodiode produces an interferogram (Fig. 2.3(e)) that can be described as a product of two FC pulses integrated over the photodiode bandwidth. This signal is usually acquired as a function of the effective time, $n\Delta T$, where n is the sample number at time intervals of ΔT [86]. A weak ringing that can be observed on the edges of the pulse (Fig. 2.3(d)) contains absorption information of the DUT.

2.4.2 Mathematical description

Mathematical analysis in this section is based on work [88]. Let us denote absolute frequencies of two FCs as $\nu_k = f_{ceo_1} + kf_{r_1}$ and $\nu_m = f_{ceo_2} + mf_{r_2}$, where $k = 0...K-1$ and $m = 0...M-1$ are the comb line numbers and f_{ceo} is a carrier-envelope-offset (CEO) frequency of the corresponding FC, comprising the carrier frequency of the laser. Then, the electric field equations of the FCs can be described as

$$E_1(t) = \sum_{k=0}^{K-1} G_k(\nu_k - \nu_c)e^{i(2\pi\nu_k t + \phi_k)} \tag{2.4}$$

and

$$E_2(t) = \sum_{m=0}^{M-1} G_m(\nu_m - \nu_c)e^{i(2\pi\nu_m t + \phi_m)}, \tag{2.5}$$

where $G_k(\nu_k - \nu_c)$ and $G_m(\nu_m - \nu_c)$ are the spectral profiles of the FCs, ν_c is the center frequency, ϕ_k and ϕ_m are the phase factors. Note that in Fig. 2.3(a,b) both FCs have ideal shape, which is not true in reality.

After the interaction of two FCs on the detector, the heterodyne

interference output voltage is given by [88]

$$U(t) \sim Re\{\sum_{k,m} \tilde{A}_k \tilde{A}_m^* e^{i(2\pi[\nu_k - \nu_m]t)}\}, \tag{2.6}$$

where $\tilde{A}_k = G_k(\nu_k - \nu_c)e^{i\phi_k}$ and $\tilde{A}_m^* = G_m(\nu_m - \nu_c)e^{i\phi_m}$ are complex amplitudes of the k^{th} and m^{th} components for corresponding FCs.

The RF frequency components after multi-heterodyne interference are defined as

$$\begin{aligned} f_k^{RF} = \nu_k - \nu_m = f_{ceo_1} + kf_{r_1} - (f_{ceo_2} + mf_{r_2}) = \\ = \Delta f_{ceo} + (k-m)f_{r_2} + k\Delta f_r = f_{ceo}^{RF} + k\Delta f_r, \end{aligned} \tag{2.7}$$

where $f_{ceo}^{RF} = \Delta f_{ceo} + (k-m)f_{r_2}$ is the artificially prescribed CEO frequency of the heterodyne comb structure, far from the zero frequency to maintain k as a common index between the combs in optical and RF domains [88]. It should be noted that $k - m$ can not exceed 1, since the detector's bandwidth is limited.

An electronic filter is applied to map each optical frequency in FC to one single RF frequency. In this case comb line numbers k and m match each other and are limited to satisfy the following inequality:

$$\frac{-f_{r_2}}{2} < f_{ceo}^{RF} + k\Delta f_r < \frac{f_{r_2}}{2}. \tag{2.8}$$

The range of k is defined by the center wavelength and bandwidth of the optical band-pass filter, and only one possible m responds to a specific value of k under the condition (2.8). Under this requirement the corresponding phases of the RF frequency components can be written as

$$\begin{aligned} \phi_k^{RF} = \phi_k - \phi_m = \phi_{01} + 2\pi\nu_k\tau_{01} - (\phi_{02} + 2\pi\nu_m\tau_{02}) = \\ = \phi_0^{RF} + 2\pi f^{RF}\tau_0^{RF}, \end{aligned} \tag{2.9}$$

where ϕ_{01}, ϕ_{02} and τ_{01}, τ_{01} are carrier envelope phases and the initial pulse center positions of two FCs respectively, ϕ_0^{RF} is the carrier envelope phase and τ_0^{RF} is the initial pulse center position of the interferograms.

The output voltage of the detector can then be simplified to

$$U(t) \sim Re\{\sum_{k=0}^{K-1} H(f_k^{RF} - f_c^{RF}) e^{i(2\pi f_k^{RF} t + \phi_k^{RF})}\}, \tag{2.10}$$

where $H(f^{RF} - f_c^{RF}) \approx G_k(\nu_k - \nu_c)G_m(\nu_m - \nu_c)$ is the RF spectrum of the interferograms, $f_c^{RF} = f_{ceo}^{RF} + \frac{\Delta f_r}{f_{r_1}}(\nu_c - f_{ceo_1})$ is a carrier frequency (center frequency) of interferograms.

If a DUT is introduced after one of the comb (as in Fig. 2.3(b)), then the shape of the corresponding comb will be changed according to the impulse response of a DUT $h(t)$ and resulting voltage will be modified as

$$U(t) \sim Re\{\sum_{k=0}^{K-1} \tilde{h}_k(t)H(f_k^{RF} - f_c^{RF})e^{i(2\pi f_k^{RF}t + \phi_k^{RF})}\}, \tag{2.11}$$

where $\tilde{h}_k(t)$ is the impulse response of the individual k-th comb line. Eq. 2.11 represents a set of interferograms (Fig. 2.3(e)), which in the frequency domain will give a set of impulse responses separated by Δf_r.

2.4.3 Experimental implementation

One of the advantages of the DCS is that it can be implemented on different platforms, for instance microcombs [89] or integrated MLLs [90] and various configurations, such as with sweeping the comb repetition rate by tuning the RF source [91, 92]. One of the most popular options is to use electro-optic FCs [93]. In contrast to mode-locked lasers, electro-optic FCs do not rely on a cavity for constructing the mode spectrum, and therefore provide flexibility in setting the center frequency and spacing between the comb lines. Since electro-optic combs are fed by a continuous wave laser, they provide mutual phase coherence in the DCS [93–96].

Figure 2.3(b) demonstrates a simple implementation example of the DCS based on electro-optic FCs. The laser is divided into two paths and feeds FCs, one of which is coupled in a DUT. If a SDM device is characterised, multiplexers at the input and demultiplexers at the output of a DUT should also be included in the setup. However, demultiplexers require fiber delays at the inputs and outputs for separation of impulse responses from different cores in time domain. If these delays are too large, it can be impossible to detect the transfer function from some of the fiber cores due to limited frequency resolution (limited range of time delays that can be captured by the DCS). Thus, a selection of fiber delays for a particular DUT should be made carefully. The resulting beating is measured with a reciever and digitized with a real-time sampling oscilloscope. The oscilloscope has to be equipped with sufficient

memory to capture the measurement data and its sampling clock has to be locked to the comb clocks [94]. In addition, an acousto-optic modulater (AOM) can be used for shifting away the downconverted center line of the comb from DC [94]. Such DCS configuration (Fig. 2.3(b)) requires a calibration process, so in a reference experiment the DUT should be removed from the signal arm. This measurement then has to be subtracted from the one with the DUT in post-processing. For each interferogram, the spectral complex amplitude is recovered through a Fourier transform process, which includes conventional tools in Fourier analysis, such as zero padding or phase unwrapping.

2.5 Swept-wavelength interferometry (SWI)

2.5.1 Operation principle

There are many measurement techniques that can be united under the basis of SWI as was discussed in the introductory chapter. Nuances of their implementation may depend on the application, but the defining element of all SWI systems is a frequency tunable source which is continuously swept across the measurement range of an interferometer. Unlike in traditional interferometry, where interference patterns are typically observed as a function of a spatial coordinate, the interferogram in SWI is captured as a function of the instantaneous optical frequency of a tunable source. The interferometer can be constructed with various geometries and tools, but in all of them the output of the sweeping source is split into two arms - a reference arm and a sample arm. The optical path length of the reference arm is usually fixed, and the sample arm may include multiple distinct paths. By performing a Fourier transform on the acquired interference pattern data, the complex transfer function and impulse response of the sample can be extracted (Fig. 2.4).

As was mentioned above, the interferogram in SWI is captured as a function of the instantaneous optical frequency of a tunable source. This point can be confusing because it is common to refer to raw data acquired by a real-time oscilloscope as time domain data, while data that is Fourier transformed is referred as frequency domain data. In SWI, however, the roles of the time domain and the frequency domain are reversed since the signal is acquired as a function of the instantaneous frequency of the laser source as it sweeps, rather than as a function of time. Moreover, the instantaneous frequency of the laser is a function of the sweeping time. Hence, one can represent the fringes captured in SWI experiments

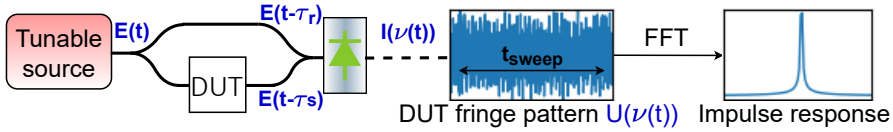

Figure 2.4: Swept wavelength interferometry implemented in a single mode optical fiber based on a Mach-Zehnder structure, showing extraction of the DUT impulse response function.

as a two-dimensional function which depends on instantaneous frequency and sweeping time, which also define a size of the measurement window of the real-time oscilloscope (see Fig. 2.4).

2.5.2 Mathematical description

In this description we consider the case of a simple interferometer based on a Mach-Zehnder geometry (Fig. 2.4). The output of the tunable laser is given as

$$E(t) = E_0 e^{-i\phi(t)} \hat{Q}, \tag{2.12}$$

where E_0 is a constant amplitude, $\hat{Q}$ is a unit polarization vector that is assumed to be constant throughout the laser sweep and $\phi(t)$ is the phase, which is related to the instantaneous frequency $\nu(t)$ of the laser as

$$\nu(t) = \frac{1}{2\pi} \frac{d\phi(t)}{dt}. \tag{2.13}$$

The instantaneous frequency $\nu(t)$ of the laser in the case of a linear frequency sweep is

$$\nu(t) = \nu_0 + \gamma t, \tag{2.14}$$

where γ is the sweep rate. Thus, by integrating Eq. (2.13), the phase is given by

$$\phi(t) = 2\pi(\nu_0 t + 0.5\gamma t^2). \tag{2.15}$$

The laser field $E(t)$ is split into two components $E(t-\tau_r)$ and $E(t-\tau_s)$ that propagate through different distances with the group delay times of the signals in the reference and sample arms τ_r and τ_s, respectively. For

simplicity an equal splitting ratio is considered. When these two components of the optical field are recombined on a photodetector, interference results in a detector voltage given by

$$U(t) = |E(t - \tau_r) + E(t - \tau_s)|^2 \tag{2.16}$$

and the final result will be

$$U(t) = U_0(1 + \cos(2\pi\gamma t\tau_0 + \psi)), \tag{2.17}$$

where $\tau_0 = \tau_s - \tau_r$, U_0 is a constant that depends on the detector sensitivity and constant amplitude E_0, and ψ is a constant phase. The result can be interpreted as a sinusoidal output for a fixed-path-length interferometer and used for a further processing and extraction of the transfer function and impulse response. In SWI it is often more convenient to represent Eq. (2.17) as a function of the instantaneous optical frequency ν, rather than a function of time:

$$U(\nu) = U_0(1 + \cos(2\pi\nu\tau_0 + \xi)), \tag{2.18}$$

where $\xi = \psi - 2\pi\nu_0\tau_0$.

In case of nonlinear frequency tuning, Eq. (2.17) can be written in a more general form of

$$U(t) = U_0(1 + \cos(\phi(t) - \phi(t - \tau_0) + \psi)). \tag{2.19}$$

In ref. [97] Eq. (2.19) is simplified by expanding $\phi(t-\tau_0)$ in a Taylor series and assuming that the instantaneous laser frequency does not change over a time interval equal to the relative delay between the interferometer arms. In this case the higher order terms in the expansion are negligible and

$$\phi(t - \tau_0) \approx 2\pi\nu(t)\tau_0, \tag{2.20}$$

so the phase difference is no longer an explicit function of time, but rather a function of the instantaneous optical frequency $\nu(t)$. After substitution of relation (2.20) in Eq. (2.19), an expression identical to Eq. (2.18) can be derived. However, in case of nonlinear tuning this equation must be applied carefully, since the fringe pattern is periodic in optical frequency, but may be aperiodical in time, whereas in the case of ideal linear tuning, the captured signal is periodic in both time and optical frequency.

2.5.3 Nonlinearity of the laser sweep and its tracking

As was mentioned in the previous section, the laser sweep is usually not perfectly linear. This leads to measurement errors and can artificially broaden the impulse response function of the DUT [97]. To overcome this issue, an auxiliary interferometer is usually introduced in the experimental setup, as indicated in Fig. 2.5(a). This interferometer assists in tracking the nonlinearity of the laser sweep, which can be then compensated [40,97,98]. One option is to linearize the nonlinear frequency sweep by extracting new sample points from the received signal of this additional interferometer. Another alternative is to use the auxiliary interferometer output as a clock signal to trigger the oscilloscope which avoids the large number of interpolations required for resampling [99–101]. Using this signal as an external clock to sample the fringe pattern output by the measurement interferometer enables sampling at equal optical frequency steps $\Delta\nu_0 = 1/\tau_0$. This, however, is correct only when the instantaneous frequency of the laser does not change significantly over τ_0 (the slow tuning approximation criterion) [97]. Along with that, the trigger signal output can be used to measure the varying laser sweep rate throughout an acquisition, providing the sweep rate data required to perform the resampling.

Both approaches discussed above rely on the condition that the interferometer output signal is periodic in optical frequency. However, when the laser sweeping speed is quite high, the slow tuning approximation is not valid anymore. Usually such lasers have significant nonlinear tuning and one can face undesired variations in the sampling interval that arise when using a particular clock to trigger the sampling of an experimental data set. Such variations are referred as sampling errors in ref [97] and have two main origins. The first appears because the frequency spacing of the output fringes is uniform only to the first order [99]. The approximation of uniform frequency spacing collapses when there is an increase in interferometer path length mismatches and average laser tuning rates. The resulting periodicity errors lead to sampling errors when the interferometer output is used as a clock for sampling swept-wavelength data sets. The second error source lies in non ideal data acquisition (DAQ) hardware in which finite optical and electronic propagation delays cause the sampled data to lag behind the clock signal by a small time interval. These delays combined with a nonlinear wavelength tuning result in a sampling grid with unequal frequency increments [102]. Such two types of sampling errors can cancel each other to second order by adding an

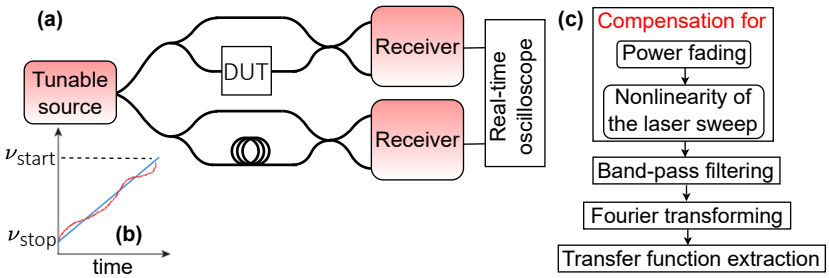

Figure 2.5: (a) Experimental setup for SWI implementation. (b) Principal sketch showing deviations (red) from the ideal linear dependence (blue) of laser's frequency on sweeping time. (c) DSP algorithm.

optical delay line into the SWI measurement system [97]. This approach allows the requirements on interferometer delay and laser tuning rate to be relaxed in the frequency sampling method.

All mentioned methods were reorganized after the developments of real-time oscilloscopes and substituted by DSP methods, but still lack absolute accuracy and suffer from a systematic error caused by a wavelength dependent fiber group delay. Owing to that, calibration of the delay arm and operation in a stable condition is required [99, 103]. Recently a new approach was reported where a FC can be used as a frequency "ruler" for such a calibration [104]. As only the repetition rate is stabilized, this technique requires the laser to sweep faster than the drift in carrier envelope offset frequencies.

2.5.4 Experimental implementation

Figure 2.5(a) shows a general experimental setup for characterisation of photonic devices using SWI. A tunable laser sweeps across the measurement range and its output is split between an interferometer with a DUT and reference interferometer assisting in tracking the nonlinearity of the laser tuning. Additional arms can be added to an experimental system for monitoring of power and polarisation fading. If the sweeping bandwidth is large enough, so that the laser experiences power fluctuations, it can assist in compensation for power fading during DSP. Finally, the signal is detected by receivers and digitized with an analog-to-digital converter (ADC).

Extraction of the transfer function and impulse response from the sampled photocurrents can be done with DSP steps shown in Fig. 2.5(c).

The first DSP module is usually devoted to the compensation for the power fading and nonlinearity of the laser sweep. Next, a bandpass filter is applied and the impulse response elements are found in the spectra obtained by Fourier transform at positions corresponding to fiber delays.

2.6 Comparison of SDM characterisation techniques

In the previous section various measurement techniques for SDM characterisation were described and reviewed. All of them have their own advantages and limitations and can be applied for different purposes depending on which parameters are measured. Depending on the considered system the performance parameters can also vary a lot and while some of the discussed methods are perfectly suitable for measurement of some devices, they can be inappropriate for others.

S^2 imaging is capable of measurement of mode shapes and DGD extraction without any demultiplexer while requires a reasonably simple setup. However, even low amount of coupling between the modes becomes detrimental for signal analysis, which makes S^2 less suitable - or at least more complex - to characterise coupled SDM devices that change with time. Moreover, the phase of the DUT is not measured in the simplest implementation of S^2 [72], making it impossible to extract a complex transfer function and calculate MDL. S^2 imaging can, however, be implemented with SWI, here the phase can be easily extracted [105].

In case of DH, in which a setup similar to S^2 is utilized, the reference beam is directed at an angle with respect to the signal, which may provide access to the phase information, even though the camera only records intensity. At the same time, DH possesses all the advantages of S^2 imaging, e.g, can assist in reconstruction of mode shapes.

The DCS is a powerful technique in terms of the resolution, measurement bandwidth and high sensitivity. Furthermore, DCS allows using both amplitude and phase information, making it possible to extract a complex transfer function of a DUT. DCS is also favorable for measurements of small dispersion values, which can be difficult to capture in short fibers [27, 93]. However, it has some limitations related to the discrete nature of the spectral comb lines. Particularly, narrow band variations that fall between the comb lines or delays that are larger than the inverse repetition rate of the combs, cannot be measured using the static DCS.

In SWI both amplitude and phase information is preserved, so the full complex transfer function can be extracted. Moreover, employing a tunable laser source enables achieving high SNR and spectral resolution. However, deviations from a linear frequency sweep and possible instability of the DUT during the sweep lead to measurement errors, which require a reference interferometer for monitoring and compensation. Overview of existing methods show that some of them can be complicated and make an experimental setup bulky.

Another technique which was not discussed in this chapter is MIMO channel equalisation [4]. The principle is that the signals from outputs of a DUT are received independently (the number of receivers correspond to the number of outputs) and then subjected to the DSP by adaptive equalisation. The equaliser adaptively learns how to invert the transmission channel and the filter weights of the equaliser (equaliser taps) contain information about the transmission channel. Equalisers updated using the minimum mean squared error or the least means squares criteria converge to the inverse of the channel transfer matrix in the noiseless regime [106]. Hence, the equaliser taps can be used to approximate the transmission channel and estimate characteristics, such as modal dispersion and MDL. However, in the presence of noise, MDL might be underestimated, which, though, can be corrected if the noise is known, as was performed in [107]. Another issue is that MIMO systems become impractical and costly for SDM-characterization of fibers with the high number of modes.

The choice of an experimental technique for SDM characterisation is always a matter of trade-offs. SWI and DCS enable capturing a full complex transfer function, but can not give the information about a mode shape that can be obtained from DH or S^2. Note that modes of multiplexer's output fibers are often different from those of transmission fibers and hence the issue is that using DCS or SWI it is not possible to measure SDM devices directly, but rather a concatenation of multiplexers, SDM device and demultiplexer. Hence, characterisation techniques that enable measurement of the optical field without demultiplexers are expected to provide more accurate results.

CHAPTER 3

Dual-Comb Swept-Wavelength Interferometry

This chapter expands the results published in [Paper A], [Paper B] and presents an experimental technique which combines DCS and SWI for photonic devices characterisation. It discusses the main concepts, experimental implementation, DSP and measurement results.

3.1 Operation principle

In the previous chapter the operation principles of DCS and SWI were described. The presented technique, DC-SWI, is a combination of these two techniques (Fig. 3.1). In DC-SWI two frequency combs with repetition rates f_{r_1} and f_{r_2} are also used, but a tunable laser is employed to simultaneously measure the intermediate frequencies over the full optical bandwidth, set by the width of the combs. In contrast to SWI, the laser is not tuned over the large bandwidth, but only covers the frequency range that corresponds to a repetition rate of the frequency comb. In principle, this corresponds to a set of parallel SWIs defined by the number of comb lines K. This practically increases the measurement speed K times compared to classic SWI and, compared to the DCS, provides continuous, rather than discrete, frequency resolution. Moreover, as the measurement trace corresponds to multiple parallel SWIs that experience the same laser sweep, we can take advantage of this to eliminate the sweep nonlinearity directly from the measurement without an ex-

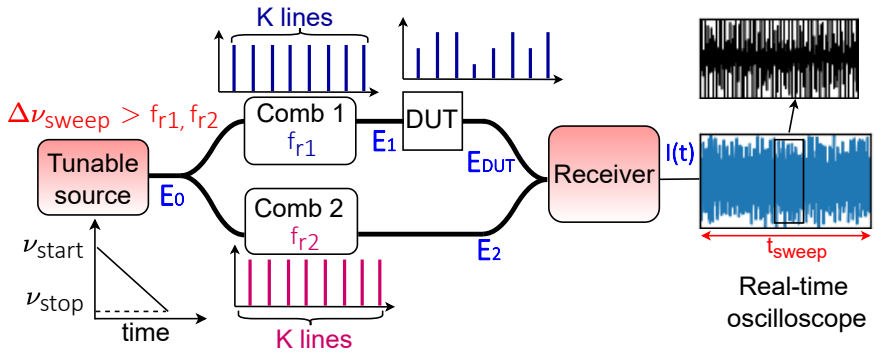

Figure 3.1: Principle of DC-SWI.

ternal calibration interferometer. It can be a beneficial point since, as discussed in sections 2.5.3 and 2.6, the process of monitoring the laser's sweep nonlinearity and its further compensation can be challenging and increases hardware complexity.

There are additional details that have to be taken into account. First, it is important to operate with a sweeping bandwidth $\Delta\nu_{sweep} = \nu_{start} - \nu_{stop}$ larger than the frequency comb spacing in order to have an overlap between the detected spectral windows, so the transfer functions from neighboring lines can be coherently stitched at the DSP stage [108]. Similarly to static DCS, the number of comb lines K and spacing Δf_r set the limitation on a sampling rate f_s, which should be no less than $K\Delta f_r$ in order to resolve all necessary spectral lines and ideally, two or more times higher. At the same time, the number of samples N should reflect the sweeping time as $N = f_s t_{sweep}$, which indicates that a real-time oscilloscope must have sufficient memory to capture the whole interferogram, as was discussed in section 2.5.1.

3.2 Mathematical description

In this section a theoretical description of the DC-SWI experimental scheme is presented.

The output electrical field of a frequency sweeping source in single polarization case can be expressed as

$$E_0(t) = A \cdot e^{-i\phi(t)}, \tag{3.1}$$

where A is a constant amplitude, $\phi(t)$ is the time-dependent phase con-

nected with an instantaneous frequency $\nu(t)$ of the laser by Eq. (2.13). Similar to the case of SWI, the phase in case of linear wavelength tuning can be expressed by Eq. (2.15). However, as was mentioned in section 2.5.3, the laser sweep is never linear in practice and this can be accounted by adding a term in Eq.(2.14), which represents the nonlinearity of the sweep. Alternatively, the phase in Eq.(3.1) can be represented by linear and nonlinear components of the laser sweep as $\phi(t) = \phi_{Lin}(t) + \phi_{NL}(t)$.

The output electrical field $E_0(t)$ of the laser is coupled to the FCs. The output of the first comb with the repetition rate f_{r_1} can be described as

$$E_1(t) = E_0(t) \sum_{k=0}^{K-1} e^{-2\pi i t \cdot k f_{r_1}}, \tag{3.2}$$

where $k = 0...K-1$ is the comb line number. Here we ignore phase profile across the comb and assume for simplicity that the modulation introduces sidebands with equal power. The second comb with the repetition rate $f_{r_2} = f_{r_1} + \Delta f_r$ is

$$E_2(t) = E_0(t) \sum_{k=0}^{K-1} e^{-2\pi i t \cdot k (f_{r_1} + \Delta f_r)}. \tag{3.3}$$

The comb in the signal arm passes through the DUT and electrical field at the output, $E_{DUT}(t)$, becomes a convolution of $E_1(t)$ with a time-domain response of the DUT $h(t)$:

$$E_{DUT}(t) = E_1(t) * h(t). \tag{3.4}$$

For simplicity we limit the mathematical description to balanced detection, however, the technique is applied equally to the case when a coherent detector is used. The fields $E_1(t)$ and $E_{DUT}(t)$ are beat on a balanced photodetector and the output photocurrent will be given by:

$$I(t) = 2R \cdot Re\{E_{DUT}(t) E_2^*(t)\}, \tag{3.5}$$

where R is the responsivity of the detector and $E_2^*(t)$ is complex conjugate of the field $E_2(t)$.

In the ideal, linear-sweep case, Eq. (3.5) can be written as

$$I(t) \sim \sum_{k=0}^{K-1} \tilde{h}_k(t) e^{-2\pi i t \cdot k \Delta f_r}, \tag{3.6}$$

where $\tilde{h}_k(t)$ is the impulse response of the individual k-th comb line. In the frequency domain this will give

$$I(\omega) \sim \sum_{k=0}^{K-1} h_k(\omega - 2\pi k \Delta f_r) \tag{3.7}$$

which is a set of K impulse responses, separated by Δf_r.

If $h(t)$ is assumed to be a simple delay, so that $h(t) = \delta(t-T)$ and $E_{DUT}(t) = E_1(t-T)$ and nonlinearity of the laser sweep is taken into account as $\phi(t) = 2\pi(\nu_0 t + 0.5\gamma t^2) + \phi_{NL}(t)$, then the Eq. (3.5) can be written as

$$\begin{aligned} I(t) = 2R \cdot Re\{ & Ae^{-i(2\pi\nu_0(t-T)+\pi\gamma(t-T)^2+\phi_{NL}(t-T))} \times \\ & \times \Big(\sum_{k=0}^{K-1} e^{-2\pi i(t-T)\cdot k f_{r_1}}\Big) \times \\ & Ae^{i(2\pi\nu_0 t+\pi\gamma t^2+\phi_{NL}(t))}\Big(\sum_{k=0}^{K-1} e^{2\pi i t\cdot k(f_{r_1}+\Delta f_r)}\Big)\} \end{aligned} \tag{3.8}$$

and after the calculation of the real part, the final expression for the photocurrent becomes

$$\begin{aligned} I(t) = 2R \cdot A^2 \sum_{k=0}^{K-1} \cos(2\pi(T\nu_0 - 0.5\gamma T^2 + Tkf_{r_1} + \\ + tk\Delta f_r + tT\gamma) + \phi_{NL}(t) - \phi_{NL}(t-T)). \end{aligned} \tag{3.9}$$

When nonlinearity of the laser tuning is negligible, the term $\phi_{NL}(t) - \phi_{NL}(t-T)$ will vanish. Moreover, one can neglect the constant terms independent of t and k and Eq. (3.9) can be simplified as

$$I(t) = 2R \cdot A^2 \sum_{k=0}^{K-1} \cos\left(2\pi(Tkf_{r_1} + tk\Delta f_r + tT\gamma)\right). \tag{3.10}$$

If the signal is sampled in time intervals Δt as $t = n\Delta t$, where $n = 1...N$ is the sample number and Δt is inverse to the sampling rate $f_s \geq K\Delta f_r$, Eq. (3.10) can be expressed in terms of the discrete samples as

$$I(n) = 2R \cdot A^2 \sum_{k=0}^{K-1} \cos\left(2\pi\left(Tkf_{r_1} + \frac{kn}{K} + n\Delta tT\gamma\right)\right), \tag{3.11}$$

which shows that the detected photocurrent contains K terms oscillating at different frequencies depending on comb line number k, and given by $k/K + T\gamma$ and offset in phase by Tkf_{r_1}. This generalizes the SWI result which is oscillations at frequency γT.

3.3 Experimental implementation

The experimental setup used in [Paper A] and [Paper B] is shown in Fig. 3.2. Two electro-optic FCs with 25.05 and 25.15 GHz repetition rates and 12 nm bandwidth (55 lines) each were used. The combs were configured with two phase modulators and one intensity modulator, with the arrangement described in detail in [94]. Agilent tunable laser that swept 25.4 GHz bandwidth in 5 ms fed the FCs. Since the modulators of the FCs have high losses, the output light from the laser was preamplified with an EDFA before entering the combs. A 25 MHz acousto-optic modulator was added for shifting away the downconverted center line of the comb from DC [94], which is not compulsory in this implementation because the signal was detected by a coherent receiver. A 25.15 GHz comb went through the DUT and 25.05 GHz comb worked as a local oscillator. The optical field was measured with a Finisar 25 GHz coherent receiver and digitized at 6.25 GS/s by Tektronix DSA 71604 real-time oscilloscope. The sampling clock of the oscilloscope was locked to the 100 MHz beat-signal of the comb clocks [94], as indicated by the dashed lines in Fig. 3.2.

Since our DC-SWI implementation is based on a static DCS configuration explained in the previous chapter, characterisation experiments require a calibration process. Hence, in order to obtain a correct device characterisation, a measurement without the DUT has to be performed and then subtracted from the one with the DUT during the DSP.

The setup is flexible with respect to experimental additions. For instance, if the sweeping bandwidth is large enough, so the laser experiences power fluctuations, a power monitoring arm can be included, the data from which can assist in power calibration during the DSP. In our experiments it was not strictly necessary since the sweeping bandwidth, which reflects the repetition rate of the FCs, was small and there were no significant fluctuations in the power level during the swep. Additionally, an auxiliary interferometer can be used for comparison of the performance when different algorithms for laser sweep nonlinearity compensation are applied.

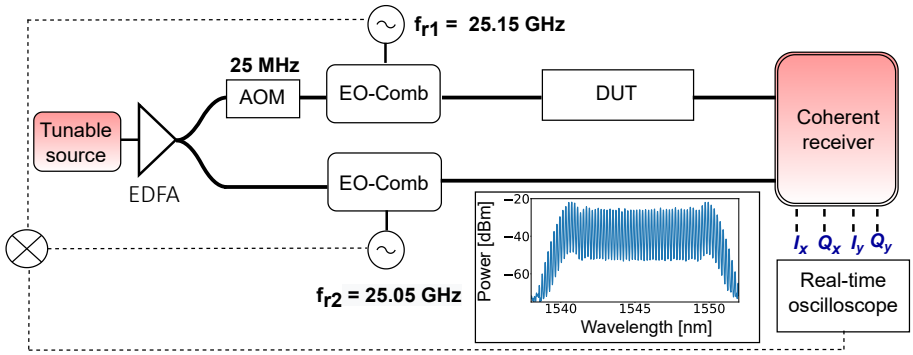

Figure 3.2: Experimental setup for characterization measurements with DC-SWI. EDFA: erbium doped fiber amplifier, AOM: acousto-optic modulator, EO-comb: electro-optic frequency comb, DUT: device under test. Inset: Optical spectrum of the frequency comb with a frequency spacing of 25.15 GHz.

The signal processing is extensively presented in the DSP section of [Paper B]. The DSP algorithm flow is shown in Fig. 3.3. It consists of several steps that resemble a combination of signal processing used for SWI and DCS. After Fourier transforming the corrected received signal $I(n)$, the scan of each comb line is selected by band-pass filtering, producing parallel SWI scans, the amount of which is equivalent to the number of comb lines K. Reducing the window size provides an SNR improvement, but the frequency resolution worsens because the number of points in every window decreases. This aspect is further discussed in section 3.5. The measured signal phase is then averaged over all comb windows to extract the nonlinear laser sweep. This averaging enables estimation of the common phase that defines the nonlinear component of the laser sweep and can be subsequently subtracted from the complex signal. A separate reference interferometer is therefore not necessary for the mitigating the laser sweep nonlinearity. The compensation procedure is flexible and can be performed using a common phase calculated only from a part of measured spectral windows or a set of particular windows if the measured DUT has drastic changes in particular comb scans. As an example of such selection, Fig. 3.4(c) demonstrates calculated phase profiles of a 22 m SMF. These curves are extracted from the same measurement, but during the DSP different number of spectral windows was used for averaging the nonlinear component of the laser's phase. The results are further discussed in section 3.4.1. After the compensation,

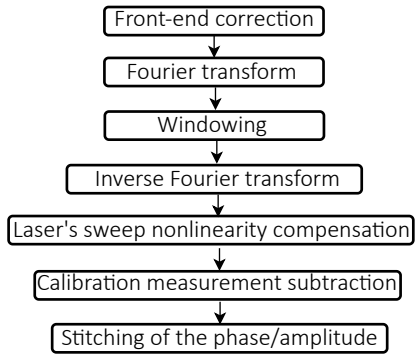

Figure 3.3: DC-SWI DSP routine flow.

calibration of each line with respect to measurement without a DUT is performed. Finally, these K traces are stitched via the overlap regions in order to produce the broadband full-field transfer function.

3.4 Experimental results

In [Paper B] several measurements using applied filters on a Finisar 1000S Waveshaper were shown in order to demonstrate the capabilities of the proposed technique. In this section characterisations of the transfer function obtained using DC-SWI for SMF and 3CCF are presented.

3.4.1 Characterisation of SMF

As a first example, a simple measurement of a 22 m SMF is presented. The experimental setup described in section 3.3 was used for the characterisation.

Figure 3.4 shows the amplitude (a) and the phase (b) of the transfer function of the SMF. The amplitude profile is constant, as expected, while exhibits noise fluctuations about 1 dB due to limited SNR. The phase profile is a parabolic function, from which the quadratic dispersion β_2 parameter can be extracted. The fitting result gives β_2 = -21.14 ps^2/km at λ = 1545 nm, which agrees well with the β_2 value for SMFs.

Fig. 3.4(c) shows several phase curves that are calculated with slightly different compensation of the laser sweep nonlinearity. Different colors indicate how many comb line windows K were used for calculation of the common phase. It can be seen that the resulted phase profiles are

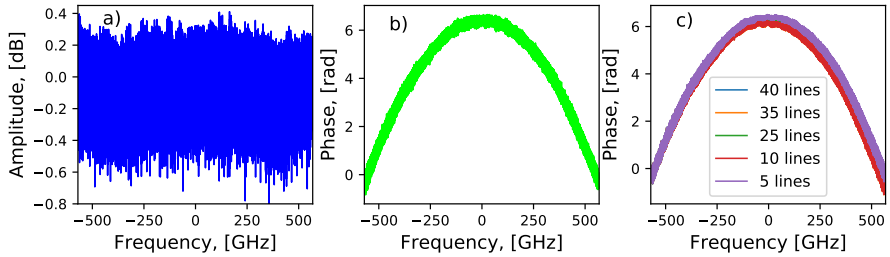

Figure 3.4: Stitched (a) amplitudes and (b) phases of the transfer function of SMF extracted from 45 comb lines. (c) Phase profiles obtained after the subtraction of the common phase calculated by averaging nonlinear laser phase components from different number of windows.

very similar and β_2 parameters for all the cases are in a good agreement with the one calculated for the case when all the comb windows phases were used for averaging (Fig. 3.4(b)). This result points out that during the DSP a flexible selection of comb spectral windows for common phase calculation can be performed.

3.4.2 Characterisation of three coupled-core fiber (3CCF)

In this section characterisation results of a 1.6 km 3CCF manufactured by Sumitomo Electric Industries are shown and discussed. These findings are mainly summaries of [Paper A] and more details can be found there.

The experimental setup for 3CCF characterisation is the same as demonstrated in Fig. 3.2 with addition of multiplexer and demultiplexer. For coupling the light into the cores of the 3CCF and handle outputs from multiple cores, fan-in/out devices based on ultrafast laser-inscribed 3D waveguides in a boro-aluminosilicate glass [109] were used.

Figure 3.5 shows plots with the magnitude of the 3CCF's transfer function over 1.1 THz comb bandwidth. The illustrated data is calculated as a sum of magnitudes of the respective X- and Y-polarizations and normalized by the total power from all the cores. Each plot corresponds to a different input fiber core. For all inputs, around 10 dB variations in maximum/minimum transmission is observed. Core 2 has slightly higher power than the other cores, which is likely due to different losses in the fan in/out devices.

Figure 3.6 represents the total power impulse responses for each fiber input core calculated as a sum of impulse responses corresponding to

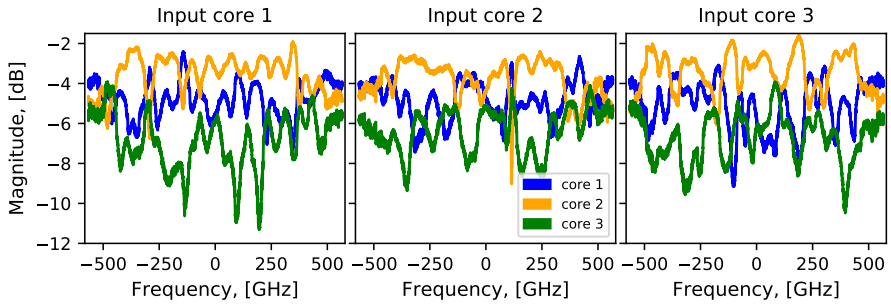

Figure 3.5: Stitched magnitudes of the transfer function extracted from 45 comb lines with light entering the different cores.

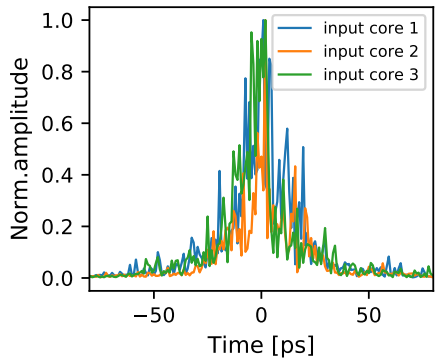

Figure 3.6: Total power impulse responses of a 1.6 km 3CCF.

output cores and then normalized by its maximum value. Possible reasons for a noisy behavior (fluctuations as a function of frequency) of the curves are reflections from fan in/out connectors or discrepancies in the phase stitching. Using values of estimated RMS widths of the impulse responses, $T_{RMS_1} = 18.9$ ps, $T_{RMS_2} = 18.6$ ps and $T_{RMS_3} = 18.5$ ps, DMGD of every fiber core can be calculated as $DMGD_i = T_{RMS_i}/\sqrt{L}$, where L is a fiber length and i is a fiber core number. Corresponding DMGDs are $\text{DMGD}_1 = 14.94$ ps/$\sqrt{\text{km}}$, $\text{DMGD}_2 = 14.65$ ps/$\sqrt{\text{km}}$ and $\text{DMGD}_3 = 14.62$ ps/$\sqrt{\text{km}}$, which are in a good agreement with properties of the CCFs that were published in [110]. These results are also consistent with previously reported values of DMGD for the 3CCF [111] and other CCFs [112].

Note that the elements of the transfer matrix were not measured simultaneously. An optical switch was used to select input core of the

3CCF during the experiment, so only 3 elements were captured per measurement shot. Input core delays can be added to enable a single-shot measurement of all inputs and outputs and this is a possible future extension of this experiment.

3.5 Discussion of performance

In this section performance characteristics, different trade-offs and competitive sides of DC-SWI are discussed.

3.5.1 Time resolution

Assuming perfect stitching and compensation for sweep nonlinearity, the time resolution, or minimum time delay δt that can be measured in DC-SWI is the inverse comb bandwidth $\Delta\nu$:

$$\delta t = \frac{1}{\Delta\nu}. \tag{3.12}$$

The comb bandwidth $\Delta\nu$, in turn, relates to the number of used spectral lines and a comb repetition rate as $\Delta\nu = K f_r$. Consequently, employing broader FCs improves the temporal resolution.

In the presented setup 50 comb lines with 25.15 GHz repetition rate were used, so the time resolution can be estimated as $\delta t \approx 0.8$ ps. This time resolution also can be reached using a static DCS or conventional SWI, since the bandwidth $\Delta\nu$ in Eq. (3.12) will be the same.

3.5.2 Frequency resolution and SNR

The frequency resolution is the minimum frequency difference between two distinct transfer function features one can distinguish. It is related to the longest delay that can be measured. In DC-SWI experiment the frequency resolution will depend on the size of the spectral window - number of points m, which is selected during the DSP. In this windowing process the number of points may decrease if only a part of the spectral window is kept, depending on the width of the impulse response. It can then be defined more generally as

$$\delta\nu = \frac{\Delta\nu}{K \cdot m} = \frac{f_r}{m}. \tag{3.13}$$

This value can be then used to calculate maximum delay time that is possible to measure, which is the inverse frequency resolution:

$$\delta T = \frac{1}{\delta \nu}. \tag{3.14}$$

In case of the processed data used in this thesis, one comb line scan contained 511 998 points before windowing, so the best possible frequency resolution in this experimental implementation can be calculated as $\delta\nu = 49.121$ kHz and the maximum delay time is 20.4 μs. Hence, the presented setup is capable of characterisation of DUTs with delays range from 0.8 ps to 20.4 μs, which is a benefit of DC-SWI because, as was pointed out in section 2.6, the spectral resolution in static DCS techniques is limited and measuring long delays can therefore be challenging.

SNR is one of the most important parameters in optical communication systems. As was discussed in [113], in DCS-based measurement schemes SNR scales per spectral line of the comb as $1/K$, while the shot-noise limited SNR in SWI will be defined only by the output power of the tunable source and the bandwidth of the detector [114]. In DC-SWI a flexible trade-off between SNR and spectral resolution is possible at the windowing stage of DSP: by selecting the desired interval around responses and cutting off unnecessary frequencies, SNR can be increased. The SNR, however, can significantly degrade when SDM devices with high core count are characterised since the number of measurement channels is increased. An appropriate choice of the power coupling ratio between reference and DUT arms of the measurement interferometer should then be considered.

A competitive advantage of DC-SWI is that one can more easily decide which trade-offs are desired during the experiment and DSP. Different comb sources and tunable lasers with various speed can be used, which also influence the capabilities of the setup and ultimate performance of the system.

CHAPTER 4

Channel models

The transfer matrix characterisation can assist not only in gaining important information about optical fibers, but also in building channel models that realistically describe their properties. A channel model can be defined as an input-output model for the given signal and is useful for estimating the transmission system performance (i.e. channel capacity) and optimising system parameters. It can also be used for developing and testing modulation formats, efficient transmission and detection schemes and in the design of photonic devices.

This chapter overviews deterministic and random models of SDM systems. The focus is on fibers with strong coupling between modes or cores since they are extensively discussed in this thesis.

4.1 Deterministic static models

Deterministic static models are based on the assumption that mode coupling is constant over time. These models usually apply coupled-mode theory [115] for characterising coupling effects and other parameters in SDM fibers. Moreover, using this approach it is possible to analyse supermodes [116, 117], which can be described as a superposition of modes from isolated cores.

In coupled mode analysis, mode coupling along a fiber with multiple

modes is described by the following equation [116]:

$$\frac{d}{dz}\mathbf{A} = -iM\mathbf{A}, \tag{4.1}$$

where $\mathbf{A} = [a_1, ..., a_N]$ is the modal amplitude vector and M is a matrix which contains propagation constants of the single mode β_0 and coefficients κ_{mn} defining the mode coupling from the m^{th} core/mode to the n^{th} core/mode. In the simplest case the coupling of m^{th} core/mode to the n^{th} core/mode is identical to the inverse coupling, so $\kappa_{mn} = \kappa_{nm}$ and in this section it is simply denoted as κ_m. For example, the case of a scalar model of a three-core fiber M when polarisation is neglected will look like

$$M = \begin{pmatrix} \beta_0 & \kappa_1 & \kappa_2 \\ \kappa_1 & \beta_0 & \kappa_3 \\ \kappa_2 & \kappa_3 & \beta_0 \end{pmatrix} \tag{4.2}$$

The solution to Eq. (4.1) can be formally written as

$$\mathbf{A}(z) = \mathbf{A}_0 \exp(iMz), \tag{4.3}$$

where exp denotes the matrix exponential and $\mathbf{A}_0$ is the input amplitude vector. Assuming a step-index fiber and the weakly-guiding approximation, the coupling coefficients can be written as [115]

$$\kappa_m = \sqrt{\frac{n_1^2 - n_2^2}{n_1^2}} \cdot \frac{1}{r} \cdot \frac{U^2}{V^3} \frac{K_0(Wd_m/r)}{K_1^2}, \tag{4.4}$$

where n_1 and n_2 are the core and cladding refractive indexes respectively, r is the core radius, d_m is a core pitch, $V = \frac{2\pi r}{\lambda_0}\sqrt{n_1^2 - n_2^2}$ is the normalized frequency, K_0 and K_1 are modified Bessel functions of order 0 and 1. Parameters U and W can be found by solving the equation system:

$$\begin{cases} U \cdot K_0(W)J_1(U) = W \cdot K_1(W)J_0(U) \\ U^2 + W^2 = V^2 \end{cases},$$

where $J_n(x)$ is the Bessel function of the first kind.

The solution (4.3) gives the opportunity to simulate the transmission and see effects of the coupling. One also can estimate DMGDs between the supermodes as has been done for 4-CCF [116] and 3CCF [118]. The study was also generalised for honeycomb multi-ring arrangements of any size in paper [79].

4.2 Models describing random coupling

The effects of random mode coupling and group delay spread in CCFs can be also evaluated by coupled-mode theory and were discussed in a recent work [119]. The coupled mode equation for the waveguide mode system in this case should account for random variations of coupling coefficients [120]. In ref. [119] these variations $\tilde{\beta}$ are assumed to be due to structural perturbations, such as bending and twisting. Eq. (4.1) in this case becomes [119]

$$\frac{d}{dz}\mathbf{A} = -i\mathbf{C}^{-1}diag(\tilde{\beta})\mathbf{C}\mathbf{A}, \tag{4.5}$$

where $\mathbf{C}$ represents the coupling matrix between the discrete core mode and coupled core mode, $diag(\tilde{\beta})$ is a diagonal matrix of elements $\tilde{\beta}_1, ...\tilde{\beta}_n$ randomly perturbed in each segment of the fiber. The accuracy of the final solution of Eq. (4.5) depends on the size of this segment, which is typically on the order of 0.1 mm for reasonable convergence [119].

The modal dispersion and its statistical properties in coupled SDM fibers can be also studied using an extension of the formalism developed for PMD [121]. The polarisation vector can be described in Jones or in 3d Stokes space [63]. Unitary operations in Jones space can be represented by rotation in Stokes space, the direction of which corresponds to the axis of rotation and its modulus equals the rotation angle. For this reason, the effect of birefringence, which is a unitary operation in Jones space, is defined by a three-dimensional rotation vector in Stokes space. The PMD can be also described using the PMD vector τ that represents birefringence-induced waveform distortion.

In order to describe a fiber with n spatial modes, the two-dimensional polarization Jones vector should be replaced by a 2n-dimensional vector. The elements of this vector represent the amplitude and phase of the various modes, and its dimension is given by $2n$ to account that every mode has two polarisation states. Similarly, the transfer matrix is transformed from 2×2 in case of single-mode transmission to $2n \times 2n$, which is generalized Jones matrix.

This can also be descried in a generalized Stokes space. Then, an extended $D = 4n^2 - 1$ dimensional Stokes space that allows the representation of multi-mode 2N-dimensional state-vectors is introduced. In this case the modal dispersion D-vector τ, as a generalised version of PMD, determines the temporal spread of propagating pulses [121]. The model was also generalised to case when MDL is present in the system [122]

and validated by comparison with experimental data.

Another type of parallelism with polarisation theory is also used in modeling. In the case of PMD, field coupling models [123] describe principal states of polarization (PSP), which are eigenvectors of a group delay operator, and are free of group delay dispersion to first order in frequency [124]. These PSPs and their group delays change in response to random changes in the amplitude and phase of the mode coupling coefficients. PSP form the basis for adaptive optical techniques to compensate PMD in direct detection systems [124].

Field coupling models have also been applied to MMF, demonstrating the existence of principal modes [125, 126], which are free of modal dispersion to first order in frequency. The existence of these modes was experimentally demonstrated in [127]. Principal modes are fundamental for adaptive optical techniques to compensate modal dispersion in direct-detection systems [128].

Coupling effects and modal dispersion are also affected by MDL. The statistical properties and system impact of MDL in the strong-coupling regime in MMFs were studied in [71, 129]. It was shown that the distribution of the modal gains is equivalent to the eigenvalue distribution of a zero-trace Gaussian unitary ensemble, which is the same as the distribution of the modal group delays [130]. The standard deviation of overall MDL depends on the standard deviation of accumulated MDL [71].

CHAPTER 5

Future outlook

There are numerous research topics related to this thesis that can be investigated in the later work. The purpose of this chapter is to briefly discuss research opportunities that are particularly connected to the work presented in Papers A and B.

Some of the advanced experimental techniques for SDM systems characterisation were discussed in chapter 2. While extensively described DCS and SWI represent many advantages, we show in [Paper A] and [Paper B] that it is beneficial to use a combination of these two schemes, DC-SWI. Application of the tunable laser source that sweeps over the comb repetition rate provides fast and accurate full-field characterization measurements without any additional interferometer for laser sweep nonlinearity compensation. The experimental results in [Paper B] demonstrate that DC-SWI enables extraction of transfer functions in a good agreement with the applied filters.

These results show that DC-SWI can be used as a tool for measuring the amplitude and phase of the transfer function and extracting the parameters of interest for various samples. Possible research opportunities unite DCS and SWI practical applications and can include metrology, optical imaging, *etc.* Moreover, the findings of [Paper A] demonstrate that DC-SWI is a promising method for characterising complex DUTs with rapid changes in transfer matrix elements. One of the possible applications in the future can be a combination of DC-SWI with an imag-

ing experimental technique in order to obtain not only the full complex transfer function, but also information about the mode shape.

Additional investigations can be carried out to improve the DC-SWI implementation in terms of the scanning speed of the intermediate frequencies. The simplest way is to use a faster tunable laser. Another scenario is to employ an arbitrary waveform generator to produce a frequency sweep in the electrical domain, similar to the arrangement in [131], which might provide more linear tuning and much higher measurement speed.

Another important application of the DC-SWI lies in the domain of channel modeling for systems based on SDM. Information gained from characterisation measurements can be used in building the complex theoretical description of the fiber optic channel model. In chapter 4 the effects of random coupling and their modeling in strongly coupled fibers were discussed. Existing models can comprehensively describe many properties, however, the a priori knowledge on time-frame changes of transfer matrix elements in a considered fiber can improve the models. The ultimate goal can be establishing a realistic dynamic model that include many rapidly changing events such a phase noise, random polarization and mode-coupling changes.

CHAPTER 6

Summary of papers

Paper A
Characterisation of a Coupled-Core Fiber Using Dual-Comb Swept-Wavelength Interferometry
Presented at European Conference on Optical Communication (ECOC), Bordeaux, France, Sep 2021.

In this paper we demonstrated transfer function measurements of the three coupled-core fiber performed with the DC-SWI, which was described in detail in [Paper B]. Using the extracted RMS-widths from the impulse response functions, values of DMGDs for every core were estimated.

Paper B
Dual-Comb Swept-Wavelength Interferometry: Theory and Experiment
Journal of Lightwave Technology, in review

In this article we comprehensively described a measurement technique which combines DCS and SWI, and demonstrated characterisation measurements over 1.25 THz bandwidth performed with the frequency resolution superior to the DCS. Experimental advantages are gained by using a tunable laser source in order to sweep over the the frequency

comb spacing and capture all intermediate frequencies. Moreover, employed DSP algorithms enabled compensation of the laser sweep without any external interferometer.

References

[1] B. I. Hirschowitz, "Photography through the fiber gastroscope," *The American journal of digestive diseases*, vol. 8, no. 5, pp. 389–395, 1963.

[2] R. S. Kerdock and D. H. Wolaver, "Atlanta fiber system experiment: results of the atlanta experiment," *The Bell System Technical Journal*, vol. 57, no. 6, pp. 1857–1879, 1978.

[3] C. E. Shannon, "A mathematical theory of communication," *The Bell System Technical Journal*, vol. 27, no. 3, pp. 379–423, 1948.

[4] R. Ryf, A. Sierra, R.-J. Essiambre, A. H. Gnauck, S. Randel, M. Esmaeelpour, S. Mumtaz, P. J. Winzer, R. Delbue, P. Pupalaikis, A. Sureka, T. Hayashi, T. Taru, and T. Sasaki, "Coherent 1200-km 6 × 6 MIMO mode-multiplexed transmission over 3-core microstructured fiber," in *37th European Conference and Exposition on Optical Communications*, 2011, p. Th.13.C.1.

[5] N. K. Fontaine, R. Ryf, H. Chen, A. V. Benitez, J. E. A. Lopez, R. A. Correa, B. Guan, B. Ercan, R. P. Scott, S. J. B. Yoo, L. Grüner-Nielsen, Y. Sun, and R. J. Lingle, "30×30 MIMO transmission over 15 spatial modes," in *Optical Fiber Communication Conference Post Deadline Papers*, 2015, p. Th5C.1.

[6] R. Ryf, N. K. Fontaine, B. Guan, R.-J. Essiambre, S. Randel, A. H. Gnauck, S. Chandrasekhar, A. Adamiecki, G. Raybon, B. Ercan, R. P. Scott, S. J. Ben Yoo, T. Hayashi, T. Nagashima, and

T. Sasaki, "1705-km transmission over coupled-core fibre supporting 6 spatial modes," in *European Conference on Optical Communication (ECOC)*, 2014, p. PD.3.2.

[7] F. P. Kapron, D. B. Keck, and R. D. Maurer, "Radiation losses in glass optical waveguides," *Applied Physics Letters*, vol. 17, no. 10, pp. 423–425, 1970.

[8] E. Chinnock, L. Cohen, W. Holden, R. Standley, and D. Keck, "The length dependence of pulse spreading in the CGW-Bell-10 optical fiber," *Proceedings of the IEEE*, vol. 61, no. 10, pp. 1499–1500, 1973.

[9] L. G. Cohen, P. Kaiser, J. B. Mac Chesney, P. B. O'Connor, and H. M. Presby, "Transmission properties of a low-loss near-parabolic-index fiber," *Applied Physics Letters*, vol. 26, no. 8, pp. 472–474, 1975.

[10] L. G. Cohen and H. M. Presby, "Shuttle pulse measurements of pulse spreading in a low loss graded-index fiber," *Applied Optics*, vol. 14, no. 6, pp. 1361–1363, 1975.

[11] D. Gloge, E. L. Chinnock, and T. P. Lee, "GaAs Twin-Laser Setup to Measure Mode and Material Dispersion in Optical Fibers," *Applied Optics*, vol. 13, no. 2, pp. 261–263, 1974.

[12] L. G. Cohen and C. Lin, "Pulse delay measurements in the zero material dispersion wavelength region for optical fibers," *Applied Optics*, vol. 16, no. 12, pp. 3136–3139, 1977.

[13] L. Cohen and C. Lin, "A universal fiber-optic (UFO) measurement system based on a near-IR fiber Raman laser," *IEEE Journal of Quantum Electronics*, vol. 14, no. 11, pp. 855–859, 1978.

[14] C. Lin, A. R. Tynes, A. Tomita, P. L. Liu, and D. L. Philen, "Chromatic dispersion measurements in single-mode fibers using picosecond InGaAsP injection lasers in the 1.2- to 1.5-μm spectral region," *The Bell System Technical Journal*, vol. 62, no. 2, pp. 457–462, 1983.

[15] K. Mori, T. Morioka, and M. Saruwatari, "Group velocity dispersion measurement using supercontinuum picosecond pulses generated in an optical fibre," *Electron. Lett*, vol. 29, no. 12, pp. 987–989, 1993.

[16] N. Nishizawa, A. Muto, and T. Goto, "Measurement of Chromatic Dispersion of Optical Fibers Using Wavelength-Tunable Soliton Pulses," *Japanese Journal of Applied Physics*, vol. 39, no. 8, pp. 4990–4992, 2000.

[17] M. Mazur, N. K. Fontaine, R. Ryf, H. Chen, and A. Blanco-Redondo, "Impulse Response Measurement of a Few-Mode Fiber Using Superconducting Nanowire Single-Photon Detectors," in *European Conference on Optical Communication (ECOC)*, 2021, p. Tu3A.3.

[18] C. Baker, Y. Lu, and X. Bao, "Chromatic-dispersion measurement by modulation phase-shift method using a Kerr phase-interrogator," *Optics Express*, vol. 22, no. 19, pp. 22 314–22 319, 2014.

[19] W. Wieser, B. R. Biedermann, T. Klein, C. M. Eigenwillig, and R. Huber, "Ultra-rapid dispersion measurement in optical fibers," *Optics Express*, vol. 17, no. 25, pp. 22 871–22 878, 2009.

[20] F. Devaux, Y. Sorel, and J. Kerdiles, "Simple measurement of fiber dispersion and of chirp parameter of intensity modulated light emitter," *Journal of Lightwave Technology*, vol. 11, no. 12, pp. 1937–1940, 1993.

[21] C. Mazzali, D. Grosz, and H. Fragnito, "Simple method for measuring dispersion and nonlinear coefficient near the zero dispersion wavelength of optical fibers," *IEEE Photonics Technology Letters*, vol. 11, no. 2, pp. 251–253, 1999.

[22] L. F. Mollenauer, P. V. Mamyshev, and M. J. Neubelt, "Method for facile and accurate measurement of optical fiber dispersion maps," *Optics Letters*, vol. 21, no. 21, pp. 1724–1726, 1996.

[23] A. L. Schawlow and C. H. Townes, "Infrared and optical masers," *Physical Review*, vol. 112, pp. 1940–1949, Dec 1958.

[24] T. H. Mainman, "Stimulated Optical Radiation in Ruby," *Nature*, vol. 187, no. 4736, pp. 493–494, 1960.

[25] A. Javan, W. R. Bennett, and D. R. Herriott, "Population inversion and continuous optical maser oscillation in a gas discharge containing a He-Ne mixture," *Physical Review Letters*, vol. 6, pp. 106–110, 1961.

[26] L. E. Hargrove, R. L. Fork, and M. A. Pollack, "Locking of He-Ne laser modes induced by synchronous intracavity modulation," *Applied Physics Letters*, vol. 5, no. 1, pp. 4–5, 1964.

[27] V. Durán, P. A. Andrekson, and V. Torres-Company, "Electro-optic dual-comb interferometry over 40 nm bandwidth," *Optics Letters*, vol. 41, no. 18, p. 4190, 2016.

[28] A. Ishizawa, T. Nishikawa, M. Yan, G. Millot, H. Gotoh, T. Hänsch, and N. Picqué, "Optical Frequency Combs of Multi-GHz Linespacing for Real-time Multi-heterodyne Spectroscopy," in *Conference on Lasers and Electro-Optics (CLEO)*, 2015, p. SW1G.7.

[29] D. A. Long, A. J. Fleisher, K. O. Douglass, S. E. Maxwell, K. Bielska, J. T. Hodges, and D. F. Plusquellic, "Multiheterodyne spectroscopy with optical frequency combs generated from a continuous-wave laser," *Optics Letters*, vol. 39, no. 9, pp. 2688–2690, 2014.

[30] V. R. Supradeepa, C. M. Long, D. E. Leaird, and A. M. Weiner, "Fast characterization of dispersion and dispersion slope of optical fiber links using spectral interferometry with frequency combs," *IEEE Photonics Technology Letters*, vol. 22, no. 3, pp. 155–157, 2010.

[31] M. Soriano-Amat, "Time-expanded phase-sensitive optical time-domain reflectometry," *Light: Science & Applications*, no. 10, pp. 1–12, 2021.

[32] A. Asahara, T. Adachi, S. Akiyama, and K. Minoshima, "Spatiotemporal Characterization of Optical Vortex Light-Wave using Hyperspectral Dual-Comb Imaging," in *Conference on Lasers and Electro-Optics (CLEO)*, 2020, p. STu4N.6.

[33] M. Mazur, N. K. Fontaine, S. Corteselli, H. Chen, L. Dallachiesa, T. Hayashi, H. Sakuma, T. Hasegawa, R. Ryf, and D. T. Neilson, "Comparison of transfer matrix stability between a 110 km 7-core coupled-core multi-core fiber and single-mode fiber," in *Optical Fiber Communications Conference and Exhibition (OFC)*, 2022, p. M1E.2.

[34] D. R. Carlson, D. D. Hickstein, and S. B. Papp, "Broadband, electro-optic, dual-comb spectrometer for linear and nonlinear

measurements," *Optics Express*, vol. 28, no. 20, pp. 29 148–29 154, 2020.

[35] E. L. Teleanu, V. Durán, and V. Torres-Company, "Electro-optic dual-comb interferometer for high-speed vibrometry," *Optics Express*, vol. 25, no. 14, pp. 16 427–16 436, 2017.

[36] P. Martín-Mateos, F. U. Khan, and O. E. Bonilla-Manrique, "Direct hyperspectral dual-comb imaging," *Optica*, vol. 7, no. 3, pp. 199–202, 2020.

[37] C. Poole, N. Bergano, R. Wagner, and H. Schulte, "Polarization dispersion and principal states in a 147-km undersea lightwave cable," *Journal of Lightwave Technology*, vol. 6, no. 7, pp. 1185–1190, 1988.

[38] B. Heffner, "Automated measurement of polarization mode dispersion using jones matrix eigenanalysis," *IEEE Photonics Technology Letters*, vol. 4, no. 9, pp. 1066–1069, 1992.

[39] W. Eickhoff and R. Ulrich, "Optical frequency domain reflectometry in single-mode fiber," *Applied Physics Letters*, vol. 39, no. 9, pp. 693–695, 1981.

[40] B. J. Soller, D. K. Gifford, M. S. Wolfe, and M. E. Froggatt, "High resolution optical frequency domain reflectometry for characterization of components and assemblies," *Optics Express*, vol. 13, no. 2, pp. 666–674, 2005.

[41] J. von der Weid, R. Passy, G. Mussi, and N. Gisin, "On the characterization of optical fiber network components with optical frequency domain reflectometry," *Journal of Lightwave Technology*, vol. 15, no. 7, pp. 1131–1141, 1997.

[42] M. Froggatt and J. Moore, "High-spatial-resolution distributed strain measurement in optical fiber with Rayleigh scatter," *Applied Optics*, vol. 37, no. 10, pp. 1735–1740, 1998.

[43] D. K. Gifford, M. E. Froggatt, and S. T. Kreger, "High precision, high sensitivity distributed displacement and temperature measurements using OFDR-based phase tracking," in *21st International Conference on Optical Fiber Sensors*, vol. 7753, 2011, pp. 536–539.

[44] D.-P. Zhou, Z. Qin, W. Li, L. Chen, and X. Bao, "Distributed vibration sensing with time-resolved optical frequency-domain reflectometry," *Optics Express*, vol. 20, no. 12, pp. 13 138–13 145, 2012.

[45] E. Baumann, F. R. Giorgetta, I. Coddington, L. C. Sinclair, K. Knabe, W. C. Swann, and N. R. Newbury, "Comb-calibrated frequency-modulated continuous-wave ladar for absolute distance measurements," *Optics Letters*, vol. 38, no. 12, pp. 2026–2028, 2013.

[46] L. E. Smith, M. Bonesi, R. Smallwood, S. J. Matcher, and S. MacNeil, "Using swept-source optical coherence tomography to monitor the formation of neo-epidermis in tissue-engineered skin," *Journal of Tissue Engineering and Regenerative Medicine*, vol. 4, no. 8, pp. 652–658, 2010.

[47] N. K. Fontaine, R. Ryf, M. A. Mestre, B. Guan, X. Palou, S. Randel, Y. Sun, L. Grüner-Nielsen, R. V. Jensen, and R. Lingle, "Characterization of Space-Division Multiplexing Systems using a Swept-Wavelength Interferometer," in *Optical Fiber Communication Conference*, 2013, p. OW1K.2.

[48] J. van Weerdenburg, S. Rommel, J. M. D. Mendinueta, W. Klaus, J. Sakaguchi, J. J. Vegas Olmos, T. Koonen, Y. Awaji, I. T. Monroy, C. Okonkwo, and N. Wada, "Enhanced Modal Dispersion Estimation Enabled by Chromatic Dispersion Compensation in Optical Vector Network Analysis," *Journal of Lightwave Technology*, vol. 37, no. 16, pp. 4001–4007, 2019.

[49] J. Carpenter, B. J. Eggleton, and J. Schröder, "Reconfigurable spatially-diverse optical vector network analyzer," *Optics Express*, vol. 22, no. 3, pp. 2706–2713, 2014.

[50] M. Mazur, N. K. Fontaine, R. Ryf, H. Chen, D. T. Neilson, M. Bigot-Astruc, F. Achten, P. Sillard, A. Amezcua-Correa, J. Schröder, and J. Carpenter, "Characterization of Long Multi-Mode Fiber Links using Digital Holography," in *Optical Fiber Communication Conference (OFC)*, 2019, p. W4C.5.

[51] J. Bohn, J. Carpenter, S. Gross, M. Withford, and J. Schröder, "Characterization of laser inscribed on-chip photonic lanterns with

different core distances," in *European Conference on Optical Communication (ECOC)*, 2015, p. P.1.14.

[52] S. Rommel, J. M. D. Mendinueta, W. Klaus, J. Sakaguchi, J. J. V. Olmos, Y. Awaji, I. T. Monroy, and N. Wada, "Few-mode fiber, splice and SDM component characterization by spatially-diverse optical vector network analysis," *Optics Express*, vol. 25, no. 19, pp. 22 347–22 361, 2017.

[53] D. Gabor, "A New Microscopic Principle," *Nature*, vol. 161, no. 4098, pp. 777–778, 1948.

[54] T. Kubota, "48 Years with holography," *Optical Review*, vol. 21, no. 6, pp. 883–892, 2014.

[55] J. W. Goodman and R. W. Lawrence, "Digital image formation from electronically detected holograms," *Applied Physics Letters*, vol. 11, no. 3, pp. 77–79, 1967.

[56] T. Tahara, X. Quan, R. Otani, Y. Takaki, and O. Matoba, "Digital holography and its multidimensional imaging applications: a review," *Microscopy*, vol. 67, no. 2, pp. 55–67, 2018.

[57] S. van der Heide, B. van Esch, M. van den Hout, T. Bradley, A. M. Velazquez-Benitez, N. K. Fontaine, R. Ryf, H. Chen, M. Mazur, J. E. Antonio-Lopez, J. C. Alvarado-Zacarias, R. Amezcua-Correa, and C. Okonkwo, "Optical Field Characterization using Off-axis Digital Holography," in *Optical Fiber Communications Conference and Exhibition (OFC)*, 2022, p. M3Z.6.

[58] J. C. Alvarado-Zacarias, N. K. Fontaine, R. Ryf, H. Chen, S. van der Heide, J. E. Antonio-Lopez, S. Wittek, G. Li, C. Okonkwo, M. Bigot-Astruc, A. Amezcua-Correa, P. Sillard, and R. Amezcua-Correa, "Assembly and characterization of a multimode edfa using digital holography," in *Optical Fiber Communication Conference (OFC)*, 2020, p. Th1H.6.

[59] Payal and S. Kumar, "Nonlinear impairments in fiber optic communication systems: Analytical review," in *Futuristic Trends in Network and Communication Technologies*, P. K. Singh, M. Paprzycki, B. Bhargava, J. K. Chhabra, N. C. Kaushal, and Y. Kumar, Eds. Singapore: Springer Singapore, 2019, pp. 28–44.

[60] G. Keiser, *Optical Signal Attenuation and Dispersion.* Springer Singapore, 2021, pp. 93–145.

[61] G. P. Agrawal, *Fiber-Optic Communication Systems*, 5th ed. Wiley, 2021.

[62] ——, *Nonlinear Fiber Optics*, 5th ed. Springer, 2013.

[63] J. N. Damask, *Polarization Optics in Telecommunications.* Springer, 2004.

[64] T. Sakamoto, T. Mori, T. Yamamoto, and S. Tomita, "Differential mode delay managed transmission line for wide-band wdm-mimo system," in *Optical Fiber Communication Conference*, 2012, p. OM2D.1.

[65] P. Sillard, D. Molin, M. Bigot-Astruc, A. Amezcua-Correa, K. de Jongh, and F. Achten, "DMGD-compensated links," in *Optical Fiber Communication Conference*, 2017, p. Tu2J.4.

[66] R. Ryf, N. K. Fontaine, S. Wittek, K. Choutagunta, M. Mazur, H. Chen, J. Carlos Alvarado-Zacarias, R. Amezcua-Correa, M. Capuzzo, R. Kopf, A. Tate, H. Safar, C. Bolle, D. T. Neilson, E. Burrows, K. Kim, M. Bigot-Astruc, F. Achten, P. Sillard, A. Amezcua-Correa, J. M. Kahn, J. Schröder, and J. Carpenter, "High-spectral-efficiency mode-multiplexed transmission over graded-index multimode fiber," in *European Conference on Optical Communication (ECOC)*, 2018, p. Th3B.1.

[67] K.-P. Ho and J. M. Kahn, "Mode coupling and its impact on spatially multiplexed systems," in *Optical Fiber Telecommunications*, 6th ed. Boston: Academic Press, 2013, pp. 491–568.

[68] X. Zhao and F. Choa, "Demonstration of 10-Gb/s transmissions over a 1.5-km-long multimode fiber using equalization techniques," *IEEE Photonics Technology Letters*, vol. 14, no. 8, pp. 1187–1189, 2002.

[69] T. Mori, T. Sakamoto, M. Wada, T. Yamamoto, F. Yamamoto, and K. Nakajima, "Experimental verification of signal quality difference induced by differential modal loss and modal crosstalk on optical mimo transmission and its compensation by equipartition multiplexing," *Journal of Lightwave Technology*, vol. 34, no. 3, pp. 918–927, 2016.

[70] K. Shibahara, T. Mizuno, D. Lee, and Y. Miyamoto, "Signal processing techniques for DMD and MDL mitigation in dense SDM transmissions," in *Optical Fiber Communication Conference*, 2017, p. M2D.3.

[71] K.-P. Ho and J. M. Kahn, "Mode-dependent loss and gain: statistics and effect on mode-division multiplexing," *Optics Express*, vol. 19, no. 17, pp. 16 612–16 635, 2011.

[72] J. W. Nicholson, A. D. Yablon, S. Ramachandran, and S. Ghalmi, "Spatially and spectrally resolved imaging of modal content in large-mode-area fibers," *Optics Express*, vol. 16, no. 10, pp. 7233–7243, 2008.

[73] S. Ramachandran, J. Nicholson, S. Ghalmi, and M. Yan, "Measurement of multipath interference in the coherent crosstalk regime," *IEEE Photonics Technology Letters*, vol. 15, no. 8, pp. 1171–1173, 2003.

[74] J. W. Nicholson, A. D. Yablon, J. M. Fini, and M. D. Mermelstein, "Measuring the Modal Content of Large-Mode-Area Fibers," *IEEE Journal of Selected Topics in Quantum Electronics*, vol. 15, no. 1, pp. 61–70, 2009.

[75] J. Bromage, J. M. Fini, C. Dorrer, and J. D. Zuegel, "Characterization and optimization of Yb-doped photonic-crystal fiber rod amplifiers using spatially resolved spectral interferometry," *Applied Optics*, vol. 50, no. 14, pp. 2001–2007, 2011.

[76] J. M. Fini, J. W. Nicholson, R. S. Windeler, E. M. Monberg, L. Meng, B. Mangan, A. DeSantolo, and F. V. DiMarcello, "Low-loss hollow-core fibers with improved single-modedness," *Optics Express*, vol. 21, no. 5, pp. 6233–6242, 2013.

[77] J. Kerttula, V. Filippov, V. Ustimchik, Y. Chamorovskiy, and O. G. Okhotnikov, "Mode evolution in long tapered fibers with high tapering ratio," *Optics Express*, vol. 20, no. 23, pp. 25 461–25 470, 2012.

[78] J. F. Bauters, M. L. Davenport, M. J. R. Heck, J. K. Doylend, A. Chen, A. W. Fang, and J. E. Bowers, "Silicon on ultra-low-loss waveguide photonic integration platform," *Optics Express*, vol. 21, no. 1, pp. 544–555, 2013.

[79] C. Xia, M. A. Eftekhar, R. A. Correa, J. E. Antonio-Lopez, A. Schülzgen, D. Christodoulides, and G. Li, "Supermodes in coupled multi-core waveguide structures," *IEEE Journal of Selected Topics in Quantum Electronics*, vol. 22, no. 2, pp. 196–207, 2016.

[80] J. Nicholson, L. Meng, J. Fini, R. Windeler, A. DeSantolo, E. Monberg, F. DiMarcello, Y. Dulashko, M. Hassan, and R. Ortiz, "Measuring higher-order modes in a low-loss, hollow-core, photonic-bandgap fiber," *Optics Express*, vol. 20, no. 18, pp. 20 494–20 505, 2012.

[81] J. W. Nicholson, J. M. Fini, A. M. DeSantolo, X. Liu, K. Feder, P. S. Westbrook, V. R. Supradeepa, E. Monberg, F. DiMarcello, R. Ortiz, C. Headley, and D. J. DiGiovanni, "Scaling the effective area of higher-order-mode erbium-doped fiber amplifiers," *Optics Express*, vol. 20, no. 22, pp. 24 575–24 584, 2012.

[82] C. Jollivet, D. Flamm, M. Duparré, and A. Schülzgen, "Detailed Characterization of Optical Fibers by Combining S^2 Imaging With Correlation Filter Mode Analysis," *Journal of Lightwave Technology*, vol. 32, no. 6, pp. 1068–1074, 2014.

[83] C. Okonkwo, M. Van Den Hout, S. van der Heide, and J. van Weerdenburg, "Fibre device estimation techniques for SDM transmission," in *European Conference on Optical Communication (ECOC)*, 2021, p. We1C2.1.

[84] M. Plöschner, T. Tyc, and T. Čižmár, "Seeing through chaos in multimode fibres," *Nature Photonics*, vol. 9, no. 8, pp. 529–535, 2015.

[85] N. K. Fontaine, R. Ryf, H. Chen, D. T. Neilson, K. Kim, and J. Carpenter, "Laguerre-Gaussian mode sorter," *Nature Communications*, vol. 10, no. 1, p. 1865, 2019.

[86] I. Coddington, N. Newbury, and W. Swann, "Dual-comb spectroscopy," *Optica*, vol. 3, no. 4, pp. 414–426, 2016.

[87] A. Parriaux, K. Hammani, and G. Millot, "Electro-optic frequency combs," *Advances in Optics and Photonics*, vol. 12, no. 1, pp. 223–287, 2020.

[88] H. Yu, K. Ni, Q. Zhou, X. Li, X. Wang, and G. Wu, "Digital error correction of dual-comb interferometer without external optical referencing information," *Optics Express*, vol. 27, no. 20, pp. 29 425–29 438, 2019.

[89] A. Shams-Ansari, M. Yu, Z. Chen, C. Reimer, M. Zhang, N. Picqué, and M. Loncar, "Microring Electro-Optic Frequency Comb Sources for Dual-Comb Spectroscopy," in *Conference on Lasers and Electro-Optics (CLEO)*, 2019, p. JTh5B.8.

[90] S. Wang, X. Fan, B. Xu, B. Wang, J. Du, and Z. He, "Hybrid dual-comb interferometer with easily established mutual coherence and a very high refresh rate," *Optics Letters*, vol. 43, no. 14, pp. 3441–3444, 2018.

[91] M. Imrul Kayes and M. Rochette, "Fourier transform spectroscopy by repetition rate sweeping of a single electro-optic frequency comb," *Optics Letters*, vol. 43, no. 5, pp. 967–970, 2018.

[92] D. R. Carlson, D. D. Hickstein, D. C. Cole, S. A. Diddams, and S. B. Papp, "Dual-comb interferometry via repetition rate switching of a single frequency comb," *Optics Letters*, vol. 43, no. 15, pp. 3614–3617, 2018.

[93] F. Ferdous, D. E. Leaird, C.-B. Huang, and A. M. Weiner, "Dual-comb electric-field cross-correlation technique for optical arbitrary waveform characterization," *Optics Letters*, vol. 34, no. 24, pp. 3875–3877, 2009.

[94] V. Durán, S. Tainta, and V. Torres-Company, "Ultrafast electrooptic dual-comb interferometry," *Optics Express*, vol. 23, no. 23, pp. 30 557–30 569, 2015.

[95] P. Martín-Mateos, B. Jerez, and P. Acedo, "Dual electro-optic optical frequency combs for multiheterodyne molecular dispersion spectroscopy," *Optics Express*, vol. 23, no. 16, pp. 21 149–21 158, 2015.

[96] G. Millot, S. Pitois, M. Yan, T. Hovhannisyan, A. Bendahmane, T. W. Hänsch, and N. Picqué, "Frequency-agile dual-comb spectroscopy," *Nature Photonics*, vol. 10, no. 1, pp. 27–30, 2016.

[97] E. D. Moore, "Advances in swept-wavelength interferometry for precision measurements," *PhD thesis*, 2011.

[98] M. Badar, P. Lu, M. Buric, and P. Ohodnicki Jr, "Integrated Auxiliary Interferometer for Self-Correction of Nonlinear Tuning in Optical Frequency Domain Reflectometry," *Journal of Lightwave Technology*, vol. 38, no. 21, pp. 6097–6103, 2020.

[99] U. Glombitza and E. Brinkmeyer, "Coherent frequency-domain reflectometry for characterization of single-mode integrated-optical waveguides," *Journal of Lightwave Technology*, vol. 11, no. 8, pp. 1377–1384, 1993.

[100] K. Takada, "High-resolution OFDR with incorporated fiber-optic frequency encoder," *IEEE Photonics Technology Letters*, vol. 4, no. 9, pp. 1069–1072, 1992.

[101] E. D. Moore and R. R. McLeod, "Correction of sampling errors due to laser tuning rate fluctuations in swept-wavelength interferometry," *Optics Express*, vol. 16, no. 17, pp. 13 139–13 149, 2008.

[102] H. Rosenfeldt, C. Knothe, J. Cierullies, and E. Brinkmeyer, "Evolution of Amplitude and Dispersion Spectra During Fiber Bragg Grating Fabrication," in *Bragg Gratings, Photosensitivity, and Poling in Glass Waveguides*, 2001, p. BWA4.

[103] S. Fujii and T. Tanabe, "Dispersion engineering and measurement of whispering gallery mode microresonator for Kerr frequency comb generation," *Nanophotonics*, vol. 9, no. 5, pp. 1087–1104, 2020.

[104] K. Twayana, Z. Ye, Óskar B. Helgason, K. Vijayan, M. Karlsson, and V. Torres-Company, "Frequency-comb-calibrated swept-wavelength interferometry," *Optics Express*, vol. 29, no. 15, pp. 24 363–24 372, 2021.

[105] J. Carpenter, B. J. Eggleton, and J. Schröder, "Spatially and temporally resolved imaging of modal content in photonic-bandgap fiber," in *Conference on Lasers and Electro-Optics (CLEO)*, 2014, p. STu3N.2.

[106] R. S. B. Ospina, C. Okonkwo, and D. A. A. Mello, "DSP-based mode-dependent loss and gain estimation in coupled SDM transmission," in *Optical Fiber Communications Conference and Exhibition (OFC)*, 2020, p. W2A.47.

[107] R. S. B. Ospina, M. van den Hout, J. C. Alvarado-Zacarias, J. E. Antonio-López, M. Bigot-Astruc, A. A. Correa, P. Sillard, R. Amezcua-Correa, C. Okonkwo, and D. A. A. Mello, "Mode-dependent loss and gain estimation in SDM transmission based on MMSE equalizers," *Journal of Lightwave Technology*, vol. 39, no. 7, pp. 1968–1975, 2021.

[108] N. K. Fontaine, R. P. Scott, L. Zhou, F. M. Soares, J. P. Heritage, and S. J. B. Yoo, "Real-time full-field arbitrary optical waveform measurement," *Nature Photonics*, vol. 4, no. 4, pp. 248–254, 2010.

[109] S. Gross and M. J. Withford, "Ultrafast-laser-inscribed 3D integrated photonics: challenges and emerging applications," *Nanophotonics*, vol. 4, no. 1, pp. 332–352, 2015.

[110] T. Hayashi and S. Tainta, "Record-Low Spatial Mode Dispersion and Ultra-Low Loss Coupled Multi-Core Fiber for Ultra-Long-Haul Transmission," *JLT*, vol. 35, no. 3, pp. 450–457, 2017.

[111] R. Ryf and R.-J. Essiambre, "Impulse Response Analysis of Coupled-Core 3-Core Fibers," in *European Conference on Optical Communications (ECOC)*, 2012, p. Mo.1.F.4.

[112] M. Mazur, N. K. Fontaine, R. Ryf, A. Marotta, H. Chen, T. Hayashi, T. Nagashima, T. Nakanishi, T. Morishima, F. Graziosi, A. Mecozzi, and C. Antonelli, "Transfer Matrix Characterization of Field-Deployed MCFs," in *European Conference on Optical Communications (ECOC)*, 2020, pp. Th1A–4.

[113] N. R. Newbury, I. Coddington, and W. Swann, "Sensitivity of coherent dual-comb spectroscopy," *Optics Express*, vol. 18, no. 8, pp. 7929–7945, 2010.

[114] M. I. Bodine, "Superresolved Swept-Wavelength Interferometry: Fundamental Limits and Use in Three-Dimensional Surface Characterization," Ph.D. thesis, University of Colorado at Boulder, 2017.

[115] A. W. Snyder, "Coupled-mode theory for optical fibers," *Journal of the Optical Society of America*, vol. 62, no. 11, pp. 1267–1277, 1972.

[116] C. Xia, N. Bai, I. Ozdur, X. Zhou, and G. Li, "Supermodes for optical transmission," *Optics Express*, vol. 19, no. 17, pp. 16 653–16 664, 2011.

[117] J. Zhou and H. Pu, "Analytical expressions for the crosstalk of super-modes in the tightly bounded multicore fibers," *Optics Express*, vol. 30, no. 4, pp. 4833–4844, 2022.

[118] C. Xia, N. Bai, R. Amezcua-Correa, E. Antonio-Lopez, A. Schulzgen, M. Richardson, X. Zhou, and G. Li, "Supermodes in strongly-coupled multi-core fibers," in *Optical Fiber Communication Conference and Exposition(OFC)*, 2013, p. OTh3K.5.

[119] K. Saitoh, "Multi-core fiber technology for SDM: Coupling mechanisms and design," *Journal of Lightwave Technology*, vol. 40, no. 5, pp. 1527–1543, 2022.

[120] T. Fujisawa and K. Saitoh, "Group delay spread analysis of strongly coupled 3-core fibers: an effect of bending and twisting," *Optics Express*, vol. 24, no. 9, pp. 9583–9591, 2016.

[121] C. Antonelli, A. Mecozzi, M. Shtaif, and P. J. Winzer, "Stokes-space analysis of modal dispersion in fibers with multiple mode transmission," *Optics Express*, vol. 20, no. 11, pp. 11 718–11 733, 2012.

[122] C. Antonelli, A. Mecozzi, M. Shtaif, N. K. Fontaine, H. Chen, and R. Ryf, "Stokes-space analysis of modal dispersion of SDM fibers with mode-dependent loss: Theory and experiments," *Journal of Lightwave Technology*, vol. 38, no. 7, pp. 1668–1677, 2020.

[123] D. Gloge, "Optical power flow in multimode fibers," *Bell System Technical Journal*, vol. 51, no. 8, pp. 1767–1783, 1972.

[124] H. Kogelnik, R. M. Jopson, and L. E. Nelson, "Polarization-mode dispersion," in *Optical Fiber Telecommunications IV-B*, 4th ed. Academic Press, 2002, pp. 725–861.

[125] M. B. Shemirani, W. Mao, R. A. Panicker, and J. M. Kahn, "Principal modes in graded-index multimode fiber in presence of spatial- and polarization-mode coupling," *Journal of Lightwave Technology*, vol. 27, no. 10, pp. 1248–1261, 2009.

[126] S. Fan and J. M. Kahn, "Principal modes in multimode waveguides," *Optics Letters*, vol. 30, no. 2, pp. 135–137, 2005.

[127] J. Carpenter, B. J. Eggleton, and S. J., "Observation of eisenbud-wigner-smith states as principal modes in multimode fibre," *Nature Photonics*, vol. 9, pp. 751–757, 2015.

[128] X. Shen, J. M. Kahn, and M. A. Horowitz, "Compensation for multimode fiber dispersion by adaptive optics," *Optics Letters*, vol. 30, no. 22, pp. 2985–2987, 2005.

[129] J. M. Kahn, K.-P. Ho, and M. B. Shemirani, "Mode coupling effects in multi-mode fibers," in *Optical Fiber Communication Conference*, 2012, p. OW3D.3.

[130] K.-P. Ho and J. M. Kahn, "Statistics of group delays in multimode fiber with strong mode coupling," *Journal of Lightwave Technology*, vol. 29, no. 21, pp. 3119–3128, 2011.

[131] F. Yang, L.-J. Zhang, Z.-Y. Zhang, X.-J. Zhou, and Y. Liu, "Nonlinearity-compensation-free optical frequency domain reflectometry based on electrically-controlled optical frequency sweep," *Journal of Electronic Science and Technology*, vol. 19, no. 1, p. 100025, 2021.

Included papers A–B

Paper A

"Characterisation of a coupled-core fiber using dual-comb swept-wavelength interferometry",
Ekaterina Deriushkina, Israel Rebolledo-Salgado, Mikael Mazur, Victor Torres-Company, Peter Andrekson, Simon Gross, Michael J. Withford, Tetsuya Hayashi, Takuji Nagashima, Jochen Schröder, and Magnus Karlsson,
European Conference on Optical Communication (ECOC), Bordeaux, France, Sep 2021.

Paper B

"Dual-comb swept-wavelength interferometry: Theory and Experiment",
Ekaterina Deriushkina, Israel Rebolledo-Salgado, Mikael Mazur, Victor Torres-Company, Peter Andrekson, Jochen Schröder, and Magnus Karlsson,
submitted in Journal of Lightwave Technology.